

# The Surface Longwave Cloud Radiative Effect derived from Space Lidar Observations

Assia Arouf<sup>1</sup>, Hélène Chepfer<sup>1</sup>, Thibault Vaillant de Guélis<sup>2,3</sup>, Marjolaine Chiriaco<sup>4</sup>, Matthew D. Shupe<sup>5,6</sup>, Rodrigo Guzman<sup>1</sup>, Artem Feofilov<sup>1</sup>, Patrick Raberanto<sup>7</sup>, Tristan S. L'Ecuyer<sup>8</sup>, Seiji Kato<sup>3</sup>, and Michael R. Gallagher<sup>5,6</sup>

<sup>1</sup>LMD/IPSL, Sorbonne Université, École Polytechnique, Institut Polytechnique de Paris, ENS, PSL Université, CNRS, Palaiseau France

<sup>2</sup>Science Systems and Applications, Inc., Hampton, Virginia, USA

<sup>3</sup>NASA Langley Research Center, Hampton, Virginia, USA

<sup>4</sup>LATMOS/IPSL, UVSQ, Université Paris-Saclay, Sorbonne Université, CNRS, 78280, Guyancourt, France

<sup>5</sup>Cooperative Institute for Research in Environmental Sciences, University of Colorado, Boulder, Colorado, USA

<sup>6</sup>NOAA Physical Sciences Laboratory, Boulder, Colorado, USA

<sup>7</sup>LMD/IPSL, CNRS, Sorbonne Université, École Polytechnique, Institut Polytechnique de Paris, ENS, PSL Université, Palaiseau France

<sup>8</sup>Department of Atmospheric and Oceanic Sciences, University of Wisconsin-Madison, USA

Correspondence to: Assia Arouf ([assia.arouf@lmd.ipsl.fr](mailto:assia.arouf@lmd.ipsl.fr))

**Abstract.** Clouds warm the surface in the longwave (LW) and this warming effect can be quantified through the surface LW cloud radiative effect (CRE). The global surface LW CRE ~~has been~~<sup>is</sup> estimated ~~over more than two decades~~ using ~~long-term observations from~~ space-based radiometers (2000–2021) ~~and over the 5-year period ending in 2011 using the combination of radar, lidar and space-based radiometer.~~ ~~but~~ Previous work comparing these two types of retrievals have shown that the ~~radiometer-based cloud amount~~ has some bias over ~~continents and icy~~ surfaces. ~~It is also estimated globally using the combination of radar, lidar and space-based radiometer over the 5-year period ending in 2011. To develop a more reliable long time series of surface LW CRE over continental and icy surfaces, Here we~~ propose new estimates of the global surface LW CRE from space-based lidar observations ~~over the 2008–2020 time period.~~ We show from 1D atmospheric column radiative transfer calculations, that surface LW CRE linearly decreases with increasing cloud altitude. These computations allow us to establish simple ~~relationships–parameterizations~~ between surface LW CRE, and five cloud properties that are well observed by the CALIPSO space-based lidar: opaque cloud cover and altitude, and thin cloud cover, altitude, and emissivity. ~~We use these relationships to retrieve the surface LW CRE at global scale over the 2008–2020 time period ( $27 \text{ Wm}^{-2}$ ).~~ We evaluate this new surface LW CRE product by comparing it to existing satellite-derived products globally on instantaneous collocated data at footprint scale and on global averages, as well as to ground-based observations at specific locations. Our estimate appears to be an improvement over others as it appropriately captures the ~~annual variability of the~~ surface LW CRE ~~annual variability~~ over bright polar surfaces and it provides a dataset ~~of~~ more than 13 years long.

## 1 Introduction

Small changes in the surface irradiance may lead to large climatological responses (Chylek et al., 2007; Kwok and Untersteiner, 2011). Therefore, quantifying irradiance at the Earth's surface is a useful step to better understand the climate system. Clouds exert a very important effect on the energy balance at the surface of the Earth through their effects on shortwave (SW) and longwave (LW) radiation. They radiatively warm the surface in the LW domain because they absorb upward LW radiation that would otherwise escape the Earth system and reemit it back towards the surface. They cool the surface in the SW domain because they reflect solar radiation back to space that would otherwise partly be absorbed by the surface. These effects are usually quantified using the surface cloud radiative effect (CRE), defined as the change in the SW and LW radiation reaching the surface induced by the presence of clouds. Globally, clouds radiatively cool the Earth's surface by  $20 \text{ W m}^{-2}$  according to Kato et al. (2018) and by  $25 \text{ W m}^{-2}$  according to L'Ecuyer et al. (2019), ~~with-where~~ the (negative) surface SW CRE cooling ~~being-is~~ two times larger in magnitude than the (positive) surface LW CRE warming. Nevertheless, in some specific regions, like at high latitudes or over the tropical ocean below persistent stratocumulus clouds, the surface LW CRE warming can be larger than the surface SW CRE cooling, ~~such~~ that the clouds exert a net radiative warming of the surface.

As an example, SW effects vanish in the winter-hemisphere polar regions, leading to positive net CRE as LW effects dominate (Henderson et al., 2013). While climate warming in the Arctic is already visible with the sea ice melting (Stroeve et al., 2011), previous works showed that clouds may exert some control on future Arctic climate trajectories (Kay et al., 2016) because they play a primary role in regulating the surface energy balance (Ramanathan et al., 1989; Curry et al., 1996, Shupe and Intrieri, 2004) which influences the surface melting (van den Broeke et al., 2009). ~~Specifically, o~~Over Greenland ~~specifically~~, van Tricht et al. (2016) showed that clouds increase the radiative fluxes into the surface and ~~could~~ therefore ~~could~~ modulate the Greenland ice sheet mass balance (van Tricht et al., 2016; Hofer et al., 2017), which is a large contributor to global sea-level rise (Shepherd et al., 2012; IPCC, 2021). In the Southern high latitudes, clouds likely exert an important role on the surface energy budget of Antarctica (Shepherd et al., 2012; Kopp et al., 2016), but their radiative impact in this region remains largely unexplored (Scott et al., 2017), in spite of the fact that Antarctica contains the largest reservoir of ice on Earth. King et al. (2015) showed large errors in Antarctic surface energy budget and surface melting rates in models and underlined the importance of improving observations of cloud radiative properties in this region.

Acquaotta et al. (2014) underlined the current urgent need to develop long term reliable and high-quality climatic time series, in order to better understand, detect, predict and react to global climate variability and change. Given the importance of the surface LW CRE and the need ~~of long time series for multi-years-time series~~, it is necessary to get reliable estimates of the surface LW CRE over multiple years, everywhere around the globe including over continents and ice-covered regions. The

main motivation for the current work is to derive a ~~long-143 year-~~time series of the global surface LW CRE that can be used to better understand the cloud property that have driven the evolution of the surface LW CRE during the last decade (Vaillant de Guélis et al., 2017b, Norris et al., 2016). This is a necessary step towards understanding how clouds might interact with the surface in the future as the climate warms (Lindzen and Choi, 2021). ~~A possible~~ The ideal way to observe cloud variability ~~everywhere~~ is to combine space radar and space lidar observations (Henderson et al., 2013), because passive sensors often struggle to distinguish clouds from the surface over continents and ice-covered regions. The launch of Cloud-Aerosol Lidar and Infrared Pathfinder Satellite Observations (CALIPSO; Winker et al., 2010) and CloudSat Profiling Radar (CPR; Stephens et al., 2008) in 2006 provided the first opportunity to incorporate information about the global vertical cloud distribution (Henderson et al., 2013) over all surface types, and ~~that~~ is an important parameter for surface LW CRE estimates from space. As CloudSat experienced a battery anomaly that limited future observations to daytime scenes only in 2011, CALIPSO's global observations collected since 2006 are the main tool to provide information on the cloud vertical distribution over more than a decade. Therefore, we retrieve the surface LW CRE from space lidar alone over 13 years.

Section 2 presents the satellite and ground-based data used in this study. In section 3, we present the method followed to retrieve the surface LW CRE from radiative transfer computations. In section 4, we present the radiative-transfer-based statistical regressions tying the surface LW CRE to cloud altitude and emissivity. In section 5, we present the new surface LW CRE retrieved from the analytical relationships and CALIPSO space-based lidar observations (cloud cover, cloud altitude, and cloud opacity). In section 6, we evaluate this new surface LW CRE product ~~against ground-based observations, and~~ in section 7 we evaluate it at footprint scale and ~~that~~ at  $2^\circ \times 2^\circ$  gridded ~~products~~ scale against existing independent surface LW CRE satellite-derived products, ~~and against ground-based observations~~. In section ~~87~~, we ~~discuss the limit of the new surface LW CRE product~~ analyze the variations of the surface LW CRE and we present a long time series of the surface LW CRE retrieved from the radiative transfer computations and space-based lidar observations. Section ~~98~~ summarizes the main results and perspectives of this work.

## 2 Data

90 This section describes the CALIPSO cloud observations used to retrieve the surface LW CRE and the independent space-based- and ground-based datasets used to evaluate it.

### 2.1 Cloud observations from CALIPSO–GOCCP

We use cloud properties from the GCM Oriented CALIPSO Cloud Product (GOCCP v3.1.2; Chepfer et al., 2010; Cesana et al., 2012; Guzman et al., 2017) over the period 2008–2020. We do not use data collected between 2006 and 2007 because the  
95 laser tilted off nadir in November 2007, which introduced some change in the CALIPSO signal. In this product (hereafter, CALIPSO–GOCCP), lidar profiles are classified into three types: clear sky profile when no cloud is detected, thin cloud profile when one or several cloud layers and a surface echo are detected, and opaque cloud profile when one or several cloud layers are detected but no surface echo is detected. Surface echo is not detected typically when the profile contains a cloud with visible optical depth  $> 3$ –5 depending on the cloud microphysical properties. The cloud base height corresponds to the  
100 lowest cloud layer detected. From this classification, five fundamental cloud properties for CRE studies are derived:

- $C_{Opaque}$ : the opaque cloud cover, i.e. the number of opaque cloud profiles divided by the total number of profiles within a  $2^\circ \times 2^\circ$  latitude longitude grid box. ( ~~$2^\circ \times 2^\circ$  latitude longitude grid~~).
- $Z_{T_{Opaque}}$ : the altitude of opaque cloud, i.e. the average between the altitude of the highest cloud layer in the profile ( $Z_{Top}$ ) and the altitude of the layer where the lidar beam is fully attenuated ( $Z_{FA}$ ) is computed for each profile, a  
105 schematic illustrating these altitudes is presented in Fig. 1. Then the gridded  $Z_{T_{Opaque}}$  is the average value of all the  $Z_{T_{Opaque}}$  profiles within a grid box.
- $C_{Thin}$ : the thin cloud cover, i.e. the number of thin cloud profiles divided by the total number of profiles within a grid box.
- $Z_{T_{Thin}}$ : the altitude of thin cloud, i.e. the average between the altitude of the highest cloud layer in the profile ( $Z_{Top}$ ) and the altitude of the lowest cloud layer ( $Z_{Base}$ ) is computed for each profile, a schematic illustrating these  
110 altitudes is presented in Fig. 1. Then the gridded  $Z_{T_{Thin}}$  is the average value of all the  $Z_{T_{Thin}}$  profiles within a grid box.
- $\varepsilon_{Thin}$ : the thin cloud emissivity, derived from the space lidar ~~measurement retrieval~~ of the thin cloud visible optical depth  $\tau_{Thin}^{VIS}$  from which we estimate the thin cloud LW optical depth  $\tau_{Thin}^{LW}$ , which is approximately half of  $\tau_{Thin}^{VIS}$  (Garnier et al., 2015). The relationship  $\varepsilon_{Thin} = 1 - e^{-\tau_{Thin}^{LW}}$  (eg. Vaillant de Guélis et al., 2017a) is computed for each  
115 profile and then averaged over all the values within a grid box.



Figure 1 presents the altitudes of interest of an opaque cloud and a thin cloud seen from a downward space-based lidar beam and from an upward ground-based lidar beam. A thin cloud (Fig. 1 left) is characterized by three altitudes:  $Z_{Top}$ ,  $Z_{Base}$  and  $Z_{T_{Thin}}$ , which is the average value of the previous two ~~ones~~. For an ideal case, ~~These~~ these three altitudes are the same when observed from a space-based lidar or a ground-based lidar ~~for an ideal case~~.

120 An opaque cloud (Fig. 1 right) is characterized by three altitudes. When the lidar is based on the ground, we measure the altitude of the lowest cloud layer ( $Z_{Base}$ ), the altitude where the lidar beam is fully attenuated ( $Z_{FA-G}$ ), and  $Z_{T_{Opaque-G}}$  which is the average of the two. When the lidar is on-board a satellite, we measure the highest cloud layer ( $Z_{Top}$ ), the altitude where the lidar beam is fully attenuated ( $Z_{FA}$ ), and the average of the two ( $Z_{T_{Opaque}}$ ).

125 Figure 2 illustrates the mean  $2^\circ \times 2^\circ$  latitude-longitude gridded values of these five variables over the period 2008–2020. At global scale, opaque clouds are more numerous (42%; Fig. 2a) than thin clouds (25%; Fig. 2b) in the GOCCP v3.1.2. Note that these numbers are different from GOCCP v3.1.1 (35% and 36% respectively) where the threshold used to detect surface echo, which influences the identification of opaque clouds, was lower because GOCCP v3.1.1 (Guzman et al., 2017) was applied only to nighttime data ~~when since~~ noise is lower during nighttime than daytime. The GOCCP v3.1.2 is applied to nighttime and daytime observations. As expected, the multi-year, annual mean opaque and thin cloud altitudes (Fig 2c, 2d) reach maxima ( $> 9$  km) in the presence of deep convective clouds over the warm pool and over tropical continents, and minima ( $< 3$  km) in subsidence regions such as over stratocumulus along the West coast of continents. The thin cloud emissivity (Fig. 2e) is larger along the ITCZ, the continental regions and around the Antarctica peninsula.

130

## 2.2 Surface LW CRE from satellites

In this subsection, we describe the already existing global surface LW CRE datasets derived from satellite measurements, against which we will evaluate our satellite new product.

135

## 2.2.1 CERES –CCCM

~~(i) CERES–EBAF. The first dataset is the Clouds and the Earth’s Radiant Energy System (CERES) Energy Balanced and Filled (EBAF)–Surface Ed4.0 product (Kato et al., 2013, 2018). CERES EBAF–Surface (hereafter, CERES–EBAF) is a monthly mean  $1^{\circ}\times 1^{\circ}$  gridded dataset derived from the CERES radiometers onboard the Aqua and Terra platforms. The Aqua satellite was flying in the same orbit as CALIPSO until September 2018. As CERES is a passive radiometer, CERES–EBAF is less reliable over ice surfaces and continents than over oceans. It is also less reliable in the presence of multi-layered clouds where the lower cloud may be obscured by the overlying cloud (Liu et al., 2010; Stubenrauch et al., 2013). This study uses the Edition 4.1 of the product, which differs by  $+0.2\text{ W m}^{-2}$  in global annual mean from the previous edition (Kato et al., 2018).~~

(ii) CERES–CCCM. This product combines Earth’s Radiant Energy System (CERES) radiometer observations of top of the atmosphere ( TOA) LW fluxes with observations from CloudSat, CALIPSO and MODIS, as well as radiative transfer calculations, to retrieve the surface LW fluxes in all sky and clear sky scenes at a resolution of the CERES Single Scanner Footprint (SSF, 20 km diameter). This product contains the surface LW CRE at CERES SSF footprint and is part of the CALIPSO, CloudSat, CERES, and MODIS Merged Product (CCCM or C3M Kato et al., 2010). This product stops in 2011 because of the CloudSat battery anomaly. This product (Version RelB1) contains the Clouds Earth’s Radiant Energy System (CERES) footprints that include ground- track of CALIPSO and CloudSat. TOA LW fluxes are derived from CERES radiance observations using Edition 2 Aqua angular distribution model. (Loeb et al. 2005, 2007). Surface LW fluxes are computed using cloud properties derived from CALIPSO, CloudSat, and MODIS. CALIOP derived cloud products are extracted from version 3 CALIPSO VFM, 0.5kmALay, and 0.5kmCLay, and 0.5kmCPro, products (Vaughan et al. 2018) and R-04 CloudSat CLDCLASS, (Sassen and Wang 2008) and CWC-RO (Austin et al. 2009) products. MODIS cloud properties are derived by the CERES MODIS cloud algorithm described in Minnis et al. (2010). Cloud boundaries derived from CALIOP at a 1/3 km resolution and cloud boundaries derived from CPR CloudSat are merged to form cloud vertical profiles by the method described in Kato et al. (2011). These cloud profiles are further merged into CERES footprints, the size of which is approximately 20 km. Temperature and humidity profiles used in flux computations are from the Goddard Earth Observing System Data Assimilation System reanalysis (GEOS, Rienecker et al. 2008). GEOS-4 is used from July 2006 through October 2007 and GEOS-5.2 is used from November 2007. Further description of the RelB1 CERES–CCCM product is given in Ham et al. (2017) and Kato et al. (2019).

### 2.2.2 2BFLX

The 2B-FLXHR-LIDAR P1\_R04 (hereafter, 2BFLX) product is derived from combined measurements of CloudSat, CALIPSO, and the MODIS radiometer (L'Ecuyer et al., 2008; Henderson et al., 2013). It takes advantage of inferred vertical profiles of cloud properties to compute surface irradiances using a broadband radiative transfer model. The dataset currently stops in 2011 when CloudSat experienced its battery anomaly. This product ~~as well as the CALIPSO-GOCCP product are~~ sensitive to retrieval errors and biases introduced by the limited spatial and temporal characteristics of CloudSat and CALIPSO. Surface fluxes derived from a combination of radar and lidar observations in 2BFLX are also less susceptible to uncertainties due to undetected multi-layered clouds and uncertainties in cloud base height than those derived primarily from passive observations (L'Ecuyer et al., 2019; Hang et al., 2019). 2BFLX surface LW CRE product (L'Ecuyer et al., 2019) is available at gridded scale as well as on instantaneous orbit file data at a resolution of the CloudSat footprint (5 km diameter).

### 2.3 Surface LW CRE from ground-based sites

As the retrieval of the surface CRE from space observations is not direct, we will evaluate the surface LW CRE retrieved from space against that derived from surface radiation measurements collected directly at ground-based sites. For this purpose, we selected three sites located in different regions.

The first site is located in the Arctic, where constraining radiative transfer is challenging with the limited cloud, [available](#) atmospheric temperature ~~profile~~ and humidity profile observations ~~that are available~~ (Kay et al., 2015), and where the surface CRE may influence the Greenland ice-cap melt (van Trich et al., 2016; Hofer et al., 2017; Shupe et al., 2013). This Summit station (Shupe et al., 2013; Gallagher et al., 2018) is located at the top of the Greenland ice cap (72.6° N–38.5° W) with an elevation of 3250 m. Summit is unique because it is the only place where we have enough observations to make a robust assessment of the surface CRE over Greenland (Lacour et al., 2018). Here, the clear sky flux is computed using a radiative transfer algorithm with measurements of temperature and humidity profiles ~~(e.g., REFs), while the all sky flux is measured directly using a pair of upward- and downward-looking pyrgeometers~~ (e.g., Shupe and Intrieri, 2004; Intrieri et al., 2002).

The second site is located in continental mid-latitudes. This Site Instrumental de Recherche par Télédétection Atmosphérique (SIRTA, Haeffelin et al., 2005; Chiriaco et al., 2018) is located in France (48.7° N–2.2° E) with an elevation of 156 m. The data are part of the Baseline Surface Radiation Network (BSRN; Ohmura et al., 1998; Driemel et al., 2018). ~~Here, the clear sky flux is computed from measurements of near surface temperature and vertical distribution of humidity (Dupont et al., 2008). At SIRTA, the clear sky flux is a parameterization made from the surface humidity, the integrated moisture content over the atmospheric column and the air temperature at 2 m. The details are given in Dupont et al. (2008) and this product has also been used in Rojas et al. (2021). The resulting clear sky uncertainty is approximately  $\pm 5 \text{ W m}^{-2}$ .~~

The third site is located in the tropical belt where clouds influence the global climate and heat transport (Loeb et al., 2016), and where extensive deep convective clouds reach the cold tropical tropopause. Here, the surface LW CRE is small since

200 much of the surface downward LW radiation originates from emission by the moist near-surface layers of the atmosphere (Prata, 1996). This Kwajalein station (KWA, Roesch et al., 2011), which is also part of BSRN, is located in the Northern Pacific Ocean (8.72° N–167.73° E) with an elevation of 10 m.

Over the 3 ground-based sites, the radiative flux measurements at the surface are carried out using two Kipp and Zonen CM22 pyrgeometers, which measure in the spectral range of 4.5–40  $\mu\text{m}$ . ~~Observations are extracted at CALIPSO satellite overpass time above these ground stations then averaged over each month.~~

205

### 3 Method

#### 3.1 Approach

Vaillant de Guélis et al. (2017a; 2017b) retrieved the TOA LW CRE from the five CALIPSO–GOCCP cloud properties presented in Fig. 2: the opaque cloud cover, the opaque cloud altitude, the thin cloud cover, the thin cloud altitude, and thin cloud emissivity. In adapting their approach to the surface instead of the TOA, we developed a method to retrieve the surface LW CRE from the same five CALIPSO–GOCCP cloud properties. The method we have developed is based on simple parameterization. This will allow us to, in a future work, more easily to decompose more easily the temporal variations of the surface LW CRE into several components in order to identify which cloud variables have driven the variations of the surface LW CRE during the last 13 years. The following physical differences exist between the surface and the

210  
215 TOADifferences in physics at the surface compared to the TOA are the followings:

##### 3.1.1 Moisture

Moisture within the boundary layer influences ~~more~~ the surface LW CRE more than the TOA LW CRE. To take moisture effects into account, we add the surface elevation in the framework of Vaillant de Guélis et al. (2017) and we consider different humidity and temperature profiles at a monthly resolution and for every 2° ~~in~~-latitude, ~~with~~-differentiating oceans from continents. Compared to the fluxes themselves, Ssmall water vapor variability ~~of water vapor~~ does not affect CRE ~~very~~ much, ~~compared to the fluxes themselves~~ as the equivalent clear sky contribution is removed from CRE. The surface LW CRE dependence on temperature and humidity profiles is shown in Sect. 4.1, 4.2, and 4.3. The impact on the results of using monthly mean humidity and temperature profiles will be discussed in Section 78.

220

##### 3.1.2 Cloud heights used for the surface LW CRE estimate

In thin clouds situation, the surface LW CRE is influenced by radiation emitted downwards by all the cloud layers contained between the cloud base ( $Z_{Base}$ ) and the cloud top ( $Z_{Top}$ ). Therefore, the surface LW CRE depends on the vertical distribution of condensed water between  $Z_{Base}$  and  $Z_{Top}$  which are measured by the lidar. Therefore, we use the averaged of both ( $Z_{T_{Thin}}$ ) to estimate the surface LW CRE from lidar observations

225

In opaque cloud situation, the surface LW CRE is influenced by radiation emitted by all the cloud layers between the cloud base ( $Z_{Base}$ ) and the altitude  $Z_{Emisv\ 1}$ , defined as the altitude where the emissivity between  $Z_{Base}$  and  $Z_{Emisv\ 1}$  is equal to one.

230

The cloud layers at altitudes higher than  $Z_{Emissv1}$  do not contribute to the surface LW CRE. Therefore, the surface LW CRE depends on the vertical distribution of condensed water between  $Z_{Base}$  and  $Z_{Emissv1}$ .

In those specific cases where the vertical distribution of condensed water is such that  $Z_{Base}$  equals  $Z_{Emissv1}$ , meaning that the  $Z_{Base}$  layer (480m thick) contains enough condensed water to get alone and make the emissivity close to 1, then the surface LW CRE is driven only by  $Z_{Base}$ . In that specific case, the lidar  $Z_{FA}$  should be used to compute the surface LW CRE, and the larger the difference between  $Z_{FA}$  and the actual  $Z_{Base}$ , the more the space base lidar surface LW CRE will be underestimated.

In all the others opaque cloud situations, where  $Z_{Base}$  is lower than  $Z_{Emissv1}$ , all the cloud layers between  $Z_{Base}$  and  $Z_{Emissv1}$  contribute to the CRE, and the relative weight of each layer depends on the detailed vertical distribution of condensed water between  $Z_{Base}$  and  $Z_{Emissv1}$ . In that case, the lidar measures  $Z_{Top}$  and  $Z_{FA}$ , and we use the average  $Z_{T_{Opaque}}$ , which is the average of  $Z_{Top}$  and  $Z_{FA}$  to estimate the surface LW CRE from lidar observations.

A schematic representing the cloud altitudes seen from space and ground lidars, and the radiative transfer computations associated with each case, are represented in Figure 3.

Figure 3.A, represents an opaque cloud seen from space-based lidar (left) and the atmospheric layers that contribute to the TOA LW fluxes (right). The bottom part of the cloud under that is not observed by the space-based lidar does not contribute to the TOA LW fluxes because the lidar fully attenuates typically once the lidar laser beam has penetrated through a cloud with emissivity larger than 0.8 (eg. Vaillant de Guélis et al., 2017a).

Figure 3.B, represents an opaque cloud seen from ground-based lidar (left) and the atmospheric layers that contribute to the surface LW fluxes (right). The top part of the cloud above that is not observed by the ground-based lidar does not contribute to the surface LW fluxes.

Figure 3.C, represents a cloud seen from space-based lidar (right) and the atmospheric layers contributing to surface LW fluxes (downward red arrows on the right). The bottom part of the cloud under that is not observed by the space-based lidar does contribute to the surface LW fluxes.

To retrieve the surface LW CRE, we could use  $Z_{Base}$  from CloudSat, but this would limit our time series to 2011 only instead of 2021, and CloudSat is not always optimal to detect cloud base in particular if it is a liquid-water cloud. We chose to use what we have access to with CALIPSO: A first option consists in using  $Z_{FA}$ , the lowest opaque cloud altitude observable by space lidar ( $Z_{FA} < 3$  km above the surface most of the time, Guzman et al., 2017), which is close to the actual cloud base height except in deep convective towers and some frontal mid-latitude clouds. A second option is to use  $Z_{T_{Opaque}}$ .

which might represent the altitude of emission of the cloud in some cases. This- second option will overestimate the mean altitude of the deep convective towers, where the downward space-based lidar beam attenuates quickly without seeing much of the cloud bottom. The bias will be larger when the cloud base temperature is far from that of  $Z_{FA}$ . Moreover, this bias will depend on the opacity of the part of the cloud lying under  $Z_{FA}$  that is not observable by space lidar.

Hereafter we describe the method with  $Z_{T_{Opaque}}$ . But afterwards, we show the results for both option 1 ( $Z_{FA}$ ) and option 2 ( $Z_{T_{Opaque}}$ ). For the sake of simplicity, hereafter we describe the method with option 1 ( $Z_{FA}$ ) and option 2 ( $Z_{T_{Opaque}}$ ). The impact of the results on using these cloud heights will be discussed in Section 7.7 and 8. only.

### 3.2 Definition of the radiative quantities

In order to get simple notation, and because we are only interested by in the CRE at the surface and in the LW domain in this study, the surface LW CRE will be simply noted  $CRE$  in the following equations.

To infer  $CRE$ , the net LW radiative fluxes over all type of scenes ( $F_{Allsky}^{net}$ ) may be compared with corresponding fluxes where the influence of clouds has been removed ( $F_{Cloudy-freesky}^{net}$ ). Then, we define the surface LW CRE as follows:

$$CRE = F_{Allsky}^{net} - F_{Cloudy-freesky}^{net} \quad (1)$$

Using downwelling ( $\downarrow$ ) and upwelling ( $\uparrow$ ) fluxes, the surface LW CRE is expressed as follow:

$$CRE = (F_{Allsky}^{\downarrow} - F_{Allsky}^{\uparrow}) - (F_{Cloudy-freesky}^{\downarrow} - F_{Cloudy-freesky}^{\uparrow}) \quad (2)$$

Rearranging the terms on the right-hand side of this equation, we get:

$$CRE = (F_{Allsky}^{\downarrow} - F_{Cloudy-freesky}^{\downarrow}) - (F_{Allsky}^{\uparrow} - F_{Cloudy-freesky}^{\uparrow}) \quad (3)$$

Which can also be expressed as:

$$CRE = CRE^{\downarrow} - CRE^{\uparrow} \quad (4)$$

Where  $CRE^{\downarrow}$  represents the surface CRE on the LW downward fluxes and  $CRE^{\uparrow}$  the surface CRE on the LW upward fluxes.  $CRE^{\uparrow}$  does not exceed  $1 \text{ W m}^{-2}$  in annual global average (Allan, 2011) and in the radiative transfer computations.

Therefore, the error in the surface properties- plays a minor role.

Nevertheless, in the LW domain, clouds can warm the surface, changing the surface temperature, which is then related to the upwelling LW radiation. This is a subtle but important issue and is dependent to some degree on the surface type (i.e., land surface will warm more than ocean). If  $CRE$  is determined in a hypothetical way, one could assume that the surface temperature is the same. However, this does not capture the full impact of the clouds. To understand the full impact of the

290 | clouds, one would need to consider the adjustments of all other parameters, most importantly ~~here being~~ the surface temperature. In this study we assume that the surface temperature is the same under clouds and clear skies, consistently with the definition used in previous satellite-derived products (e.g., Kato et al., 2018; L’Ecuyer et al., 2019).

~~Thanks to the CALIPSO-GOCCP data, it is possible to decompose the surface LW CRE into contributions due to opaque clouds and thin clouds~~

295 | 
$$\dots \dots \dots (5)$$

### 3.3 Radiative transfer simulations

We use a radiative transfer code to compute the surface LW CRE due to an opaque cloud ( $CRE_{Opaque}$ ) or an optically thin cloud ( $CRE_{Thin}$ ) in an atmospheric column fully overcast by that cloud. In these 1D atmospheric columns, molecules and clouds are evenly distributed within each layer and each layer is considered infinite and homogeneous. For a single column fully overcast by an opaque cloud, we ~~establish derived the a relationship parameterization~~ between  $CRE_{Opaque}$  and the opaque cloud altitude  $Z_{T_{Opaque}}$  (see Sect. 2.1). For the single column fully overcast by a thin cloud, we ~~establish derived the a relationship parameterization~~ between  $CRE_{Thin}$ , the thin cloud altitude  $Z_{T_{Thin}}$  (see Sect. 2.1) and the thin cloud emissivity  $\epsilon_{Thin}$  as in Vaillant de Guélis et al. (2017)

305 | The radiative transfer simulations are performed with GAME (Dubuisson et al., 2004). This radiative transfer code computes LW fluxes at ~~540~~ different levels with a vertical resolution of 1 km ~~in the 25 first levels~~. The fluxes are spectrally integrated between 5 and 200  $\mu\text{m}$  consistently with CERES measurements. We prescribe various surface temperatures and the atmospheric profiles of humidity, temperature, ozone and pressure based on ERA Interim reanalysis (Dee et al., 2011) over oceans and lands for each month and latitude. Humidity and temperature profiles over land for January are presented in figure A2 in Appendix A. Figure A3 presents the seasonal and latitudinal behavior of the first layer of the humidity and temperature profiles (from the surface to 1 km above the surface) over ocean and over land. We ~~also~~ perform ~~all sky fluxes through~~ radiative transfer computations for numerous combinations of cloud opacity and vertical distribution. We prescribe the vertical extent of each cloud, the effective size of cloud particles and the infrared optical thickness. For a column fully overcast by an opaque cloud, the cloud is represented by a 1 km thick cloud layer with an emissivity equal to 1 at  $Z_{FA-G}$  ( $Z_{Top}$ ) above optically uniform cloud layers for different vertical extents with vertically integrated emissivity equal to 0.8. For a column fully overcast by a thin cloud, the cloud is represented by optically uniform cloud layers with vertically integrated emissivities equal to 0.1, 0.3, 0.5, or 0.7. The cloud top altitude varies according to latitude and can reach 17 km in tropical regions and only 11 km in polar regions. For instance, the cloud top altitude at a latitude of 39° N takes 11 different values ranging between 2 km and 13 km, and for each cloud top value, the cloud base altitude takes all possible values between 1



320 km above the surface and the cloud top altitude minus 1 km. Clear sky fluxes are defined by recalculating fluxes after removing clouds with the same humidity and temperature profiles.

### 3.4 Retrieval of surface LW cloud radiative effect from CALIPSO observations and radiative transfer simulations

The surface LW CRE is retrieved from parameterizations ~~a theoretical expression~~ derived from radiative transfer simulations that involves five observed CALIPSO–GOCCP cloud properties ~~(see Sect. 4)~~. Two surface LW CRE datasets are built from  
325 CALIPSO–GOCCP observations using this theoretical relationship over the 2008–2020 period. An orbit dataset at the CALIOP footprint resolution of instantaneous cloud property observations and a  $2^\circ \times 2^\circ$  gridded dataset of mean cloud properties. For the orbit data set, each lidar profile contains either an opaque or thin cloud or no cloud, and the surface LW CRE for this last category is zero. For the gridded product, at each grid point, the opaque surface LW CRE is computed from the gridded  $Z_{T_{Opaque}}$  and weighted by the gridded opaque cloud cover  $C_{Opaque}$  in the same way as Vaillant-de-Guélis et al.  
330 (2017). The thin surface LW CRE is computed from the gridded  $Z_{T_{Thin}}$  and gridded  $\epsilon_{Thin}$  and then weighted by the gridded thin cloud cover  $C_{Thin}$ . The total gridded surface LW CRE is the sum of the two.

$$CRE = CRE_{Opaque} + CRE_{Thin}, \quad (5)$$

335 In the retrievals, we tested both  $Z_{FA}$  and  $Z_{T_{Opaque}}$  for estimating the mean altitude of opaque clouds (as discussed in Sect. 3.1). ~~An evaluation of the retrievals against independent datasets (Sect. 5) suggests that  $Z_{T_{Opaque}}$  leads to retrievals that are similar to other space borne retrievals while  $Z_{FA}$  leads to better agreement with ground base retrievals (Sect. 6).~~

#### 4 Modeled CRE sensitivity to cloud properties

This section establishes parameterizations of the surface LW CRE against cloud altitude and emissivity over a single cloudy column using radiative transfer computations (Sect. 4.1). Then it analyzes the sensitivity of the surface LW CRE to the humidity and temperature profiles (Sect. 4.2), and to the surface elevation (Sect. 4.3).

##### 4.1 Sensitivity of the CRE to cloud altitude

Figure 43 shows the results of numerous simulations for the opaque cloud column (Fig. 43a) and the thin cloud column (Fig. 43b) for a specific atmospheric state over oceans in January at a latitude of 39° N.  $CRE_{Opaque}$  decreases approximately linearly with opaque cloud altitude at a rate of  $-6 \text{ W m}^{-2} \text{ km}^{-1}$  in this atmospheric state. This figure shows that the surface LW cloud radiative effect depends mostly on the mean altitude of the cloud and only weakly on the detailed vertical cloud distribution and the cloud bottom altitude.  $CRE_{Thin}$  also decreases linearly with thin cloud altitude, and the rate of decrease depends linearly on the cloud emissivity. The linearity of these relationships is consistent with Ramanathan et al. (1977) and Vaillant de Guélis et al. (2017, 2018). It is an empirical relation derived from radiative transfer calculations that has been verified in the observation at the TOA in Vaillant de Guélis et al. (2017a, 2018).-Corti and Peter (ACP 2009) also derived an empirical relationship (power laws) from radiative transfer computation. Our linear relationship can be seen as an approximation of the Corti and Peter (2009) power law.

Based on a regression, we obtain the following linear relationships between the surface LW CRE and cloud altitude and emissivity:

$$CRE_{Opaque} = C_{Opaque} \left[ a(RH, T) Z_{T_{Opaque}} + b(RH, T) \right] \quad (6)$$

$$CRE_{Thin} = C_{Thin} (\epsilon_{Thin} + 0.06) \left[ a(RH, T) Z_{T_{Thin}} + b(RH, T) \right] \quad (7)$$

Where  $a(RH, T)$  and  $b(RH, T)$  are constants whose values depend on the humidity and temperature profiles as discussed hereafter. For the specific case presented in Fig. 43,  $a = -6$  and  $b = 88$ .

## 365 4.2 Sensitivity of the CRE to humidity and temperature profiles

The temperature and humidity profiles in the first layers of the atmosphere largely vary according to seasons and location as presented in Fig. A3 in appendix A. ~~Since~~As these are variables that influence the surface LW CRE, their variations must be taken into account in order to retrieve the global surface LW CRE.

As an example, Figure 54.a presents the ~~Opaque~~ surface LW ~~Opaque~~ CRE for a standard humidity profile and Figure 54.b  
370 presents the ~~Opaque~~ surface LW ~~Opaque~~ CRE for an enhanced humidity profile (shown in Fig. A4). A 10% change in humidity in the first few km of the tropical atmosphere leads to a surface LW CRE change of  $7.7 \text{ W m}^{-2}$  for a cloud at 1 km and by  $5 \text{ W m}^{-2}$  for a cloud at 4 km. To capture some variability of humidity and temperature, we have established similar relationships as in Fig. 43 for each month and latitude (each  $2^\circ$ ) over land and ocean. As an example, Figure A1 shows the simulations for cloud columns for an atmospheric state over land in January at a latitude of  $39^\circ \text{ N}$  (same as Fig. 43 but over  
375 land instead of ocean). At this latitude, the amount of humidity is lower over land than ocean, therefore the LW  $F_{\text{Cloudy-freesky}}^{\text{net}}$  over land is lower and the surface LW CRE would be larger than over the ocean. The surface LW CRE is greater than that over ocean and decreases with a rate ( $a(RH,T)$ ) of  $6.5 \text{ W m}^{-2} \text{ km}^{-1}$  instead of  $6 \text{ W m}^{-2} \text{ km}^{-1}$  over ocean. Figure 65 presents the latitudinal and seasonal behavior of the linear regression coefficients ( $a(RH,T)$  and  $b(RH,T)$ ). The shape of these coefficients' spatio-temporal variation is influenced by the shape of the seasonal cycle of humidity and  
380 temperature in the first layers of the atmosphere (Fig. A3). For instance, the behavior of the intercept ( $b(RH,T)$ ) over ocean and land (Fig. 65b and Fig. 65d, respectively) is driven by the shape of the humidity amount where the largest humidity amount (in tropical regions) causes the smallest intercept coefficients. The seasonal cycle of the surface LW CRE is more pronounced over land than over ocean because the seasonal cycles of humidity and temperature are more pronounced over land than over ocean due to the heat capacity of the surface (Chepfer et al., 2019).

## 385 4.3 Sensitivity of the CRE to surface elevation

~~In order to~~To take ~~into account~~the surface elevation in the simulation into account, we consider ~~that~~the surface temperature ~~to be~~is the temperature of the atmospheric layer located at the same altitude as the surface elevation with respect to sea level, and we discard all ~~the~~layers located between ~~the~~sea level and the altitude of surface elevation~~-altitude~~. ~~We then we~~  
performed numerous radiative transfer simulations corresponding to different clouds, as described in section 3.2.

390 The results presented in Figure 76 show the sensitivity of the surface LW CRE to the surface elevation over continents in January at ~~a latitude of~~  $39^\circ \text{ N}$ . As the surface elevation increases, the atmosphere is dryer so the  $F_{\text{Cloudy-freesky}}^{\text{net}}$  decreases, and the surface LW CRE increases. The same cloud with the same cloud properties (i.e., same altitude and emissivity) will warm a surface with a high elevation more than a low elevation. For instance, an opaque cloud at an altitude of 5.5 km msl (mean sea level)~~-~~ will warm a surface at sea level by  $58 \text{ W m}^{-2}$  and a surface with an elevation of 4 km msl by  $102 \text{ W m}^{-2}$ .  
395 These results are consistent with Wang et al. (2019) who found that the surface LW CRE increases over Summit station in

Greenland due to the dry atmosphere at high elevations. We performed radiative transfer simulations for different surface elevations at all latitudes and months (not shown) and used these to retrieve the surface LW CRE from space-based lidar observations over land. Thus, the regression coefficients over land depend ~~in addition~~also on surface elevation, with a 100 m resolution ( $a(RH, T, SE)$ ,  $b(RH, T, SE)$ ).

400

## 5 New CALIPSO–GOCCP surface LW cloud radiative effect

### 5.1 Orbit Product

Figure 87 (top panel) shows the CALIPSO–GOCCP cloud vertical mask (Guzman et al., 2017) for two different parts of an orbit, both in the tropical region. The blue areas over green areas represent the opaque clouds. The blue areas over white areas represent thin clouds. The second line represents the instantaneous surface LW CRE derived from CALIPSO–GOCCP instantaneous cloud properties (opaque cloud altitude, thin cloud altitude and emissivity;  $CRE_{GOCCP}$ ), as described in Sect. 3.3. As expected, the surface LW CRE is larger for opaque clouds (Fig. 87a,  $\sim 22 \text{ W m}^{-2}$ ) than for thin clouds (Fig. 87b,  $\sim 5 \text{ W m}^{-2}$ ) for almost the same atmosphere.

### 5.2 Gridded Product

Figure 98a shows the map of the surface LW CRE derived from CALIPSO–GOCCP observations ( $CRE_{GOCCP}$ ) over the 2008–2020 time period.

In annual global means, clouds radiatively warm the surface in the LW domain by  $27 \text{ W m}^{-2}$ .  $CRE_{GOCCP}$  is maximal in the Southern Ocean ( $50\text{--}65 \text{ W m}^{-2}$ ) where the warm opaque low clouds are numerous, as already stated by L’Ecuyer et al. (2019) and Henderson et al. (2013). There are also particularly high values in the North Atlantic also has particularly high values ( $> 55 \text{ W m}^{-2}$ ), observed between Svalbard and Greenland. In the tropics, clouds typically radiatively warm the surface in the LW domain by only  $15 \text{ W m}^{-2}$ . The moist tropical oceanic atmosphere enhances the downward clear-sky fluxes, which decreases the surface LW CRE over these oceans. The maximum tropical  $CRE_{GOCCP}$  ( $30$  to  $40 \text{ W m}^{-2}$ ) is produced by warm opaque low oceanic stratocumulus clouds along the west coast of the continents.

Over continents, the weakest  $CRE_{GOCCP}$  ( $< 5 \text{ W m}^{-2}$ ) occurs over Wadi Abadi basin in the Egyptian desert ( $25^\circ \text{ N}$ ,  $33^\circ \text{ E}$ ), a cloud free region most of the time (80%). The largest  $CRE_{GOCCP}$  ( $60\text{--}65 \text{ W m}^{-2}$ ) occurs over the Tibet Autonomous Region ( $29^\circ \text{ N}$ ,  $97^\circ \text{ E}$ ), where the opaque cloud cover is high (58%) and the mean surface elevation is high (4.42 km) over 2.5 million  $\text{km}^2$ . Here, the high amount of moisture is uplifted toward southern Tibet, amplified by Rayleigh distillation as the vapor moves over the Himalayan mountains (He et al., 2015), which enhances the formation of opaque clouds.

CALIPSO space-based lidar differentiates well opaque clouds from thin clouds. Therefore, we can decompose the surface LW CRE derived from CALIPSO–GOCCP observations into contributions due to opaque clouds ( $CRE_{Opaque}$ ; Fig. 98b) and thin clouds ( $CRE_{Thin}$ ; Fig. 98c). This decomposition shows that 85% ( $23 \text{ W m}^{-2}$ ) of the overall annual global mean  $CRE_{GOCCP}$  ( $27 \text{ W m}^{-2}$ ) is produced by opaque clouds. Their effect is maximal ( $50\text{--}55 \text{ W m}^{-2}$ ) over the extra-tropical oceans ( $60^\circ \text{ S}$  and  $60^\circ \text{ N}$ ) where low warm opaque clouds are numerous. Thin clouds contribute only 15% ( $4 \text{ W m}^{-2}$ ) to the global

|  $CRE_{GOCCP}$ , and their effect is maximal ( $\sim 13 \text{ W m}^{-2}$ ) over the dry ~~land-~~continental polar regions of the Greenland and  
430 Antarctic ice sheets, where the thin cloud cover is large ( $\sim 40\%$ ).

|

## 6. Evaluation of the new surface LW cloud radiative effect against ground-based stations

### 6.1).-Method

435 Comparisons between ground-based measurements and the satellite-derived products ( $CRE_{GOCCP}$ ,  $CRE_{2BFLX}$ ) provide a direct evaluation of the satellite retrievals, but are limited by the difference in the spatial resolution of the satellite-derived product ( $2^\circ \times 2^\circ$ ) and the ground station observations (a few meters). For the satellite retrievals, we extract the monthly  $2^\circ \times 2^\circ$  grid box centered ~~at on~~ each ground site. For the ground-based observations, we extract the hourly observation at CALIPSO satellite overpass time above each ground site (two observations per day), ~~and then averaged~~ over each month.

440 We consider ~~all~~ days of each month, even if CALIPSO has no sampling over the site because there are only a few days where CALIPSO observations are not available (e.g., 18 days in 2008). Moreover, in this study, we are interested in an accurate representation of the surface LW CRE inter-annual variability, that might have significant impacts on climate-relevant processes, and not only in an accurate representation of the anomalies observed ~~like in e.g.~~ Rutan et al., (2015). That CALIPSO is missing some sampling over the ground-based site will likely ~~not~~ ~~change~~ significantly affect the inter-annual

445 variability (i.e. months of maxima / minima of the surface LW CRE). The locations of the three ground-based sites are reported in the maps (stars in Fig. 12e4).

### 6.2) Time series

Over the Summit Station Greenland site, on average compared to ground-based observations, CALIPSO-GOCCP

450 underestimates the surface LW CRE by  $8.5 \text{ W m}^{-2}$ , while 2BFLX underestimates it by  $16.4 \text{ W m}^{-2}$  and CERES-EBAF overestimates it by  $36.6 \text{ W m}^{-2}$  (Fig. 139a). The comparison of averages is made only when all products are available and for the Greenland site, ~~this~~ which is just for three months (JFM 2011). Averages over the 2008–2010 and 2011–20165 periods (Fig. 1410) show that these biases calculated for a short period are similar to the longer periods. Over the 2008–2011 time period,  $CRE_{GOCCP}$  is close to  $CRE_{2BFLX}$  and both show consistent summer maxima and winter minima, with 2BFLX ~~being~~ slightly smaller

455 than CALIPSO-GOCCP ( $0.8 \text{ W m}^{-2}$ ). ~~follows a different annual cycle with maxima wider and shifted by about two to six months.~~ Over the 2011–20165 time period,  $CRE_{GOCCP}$  and the ground station data show similar annual cycles and CALIPSO-GOCCP remains smaller than the Greenland site ( $13.0 \text{ W m}^{-2}$ ), while the annual cycle continues to be shifted by two to four months and generally has different annual variability compared to ground station. The same behavior where CERES-EBAF overestimates the surface LW CRE comparing to CALIPSO-GOCCP is observed over the map of difference

460 (Fig. 12a) in icy polar regions, for instance over Greenland and Antarctica ice sheet. While this comparison suggests that CALIPSO-GOCCP could be biased somewhat low compared to the ground-station perspective over Greenland, it is also

clear that this approach ~~does appropriately captures~~ the annual variability, while the CERES-EBAF approach appears to be significantly biased high with an unrealistic annual cycle with a correlation coefficient between the CALIPSO-GOCCP and ground base site of 0.69 and RMSE of  $15.9 \text{ W m}^{-2}$ . The retrieval using  $Z_{FA}$  instead of  $Z_{T_{Opaque}}$  seems to compare ~~more favorably~~ to the Greenland ground-based observations ~~more favorably~~ (correlation coefficient of 0.70 and RMSE of  $15.0 \text{ W m}^{-2}$ )

Over the mid-latitude continental site (Fig. ~~139b~~) on average, CALIPSO-GOCCP underestimates the surface LW CRE by  $5.7 \text{ W m}^{-2}$  compared to ground-based observations with a correlation coefficient of 0.73 and RMSE of  $11.0 \text{ W m}^{-2}$ , while 2BFLX underestimates it by  $9.4 \text{ W m}^{-2}$  and CERES-EBAF underestimates it by  $12.1$  with a correlation coefficient of 0.67 and RMSE of  $15.5 \text{ W m}^{-2}$ .

Over the tropical ocean site (Fig. ~~139c~~) on average, CALIPSO-GOCCP underestimates the surface LW CRE by  $2.3 \text{ W m}^{-2}$  compared to ground-based observations ~~and~~, while CERES-EBAF underestimates it by  $2.7 \text{ W m}^{-2}$  and 2BFLX underestimates it by  $4.1 \text{ W m}^{-2}$ . This same behavior is found on the map of differences between  $CRE_{GOCCP}$  and  $CRE_{2BFLX}$  (Fig. ~~1254~~) along the tropical Pacific and tropical Atlantic oceans where 2BFLX underestimates the surface LW CRE comparing to CALIPSO-GOCCP.

### 6.3) Seasonal cycle

Figure ~~1410~~ presents the comparison of seasonal cycles between the satellite retrievals and the ground-based observations.

Over the Greenland site (Fig. ~~140a,d~~), CALIPSO-GOCCP and 2BFLX find the same seasonal cycle of the surface LW CRE with maxima in July, that correspond to the maximum opaque cloud cover, same as the ground-based seasonal cycle. The CERES-EBAF retrieval maximum is shifted by about three months (October, Fig. ~~14a,d~~), to a time of year that shows the minimum opaque cloud cover based on CALIPSO-GOCCP (not shown). This result suggests that during these months the CERES-EBAF retrieval does not successfully distinguish LW upward fluxes from clouds and the surface. This is consistent with CERES-EBAF low-mid and high-mid cloud fractions being biased high over the Summit site except for summer time (not shown). Consistently, Figure ~~14d~~ shows CERES-EBAF's surface LW CRE is overestimated compared to ground-base retrievals in all season except summer. As a consequence CERES-EBAF does not capture the surface LW CRE annual cycle, contrarily to CALIPSO-GOCCP and 2BFLX retrievals.

Over the mid-latitude continental site (Fig. ~~140b,e~~), the surface LW CRE seasonal cycle of CALIPSO-GOCCP and 2BFLX are close to each other and the ~~three~~two satellite-derived products show similar seasonal cycles as the ground station.

Over the tropical ocean site (Fig. ~~140c,f~~), the surface LW CRE seasonal cycle is relatively flat.



#### 6.4) Diurnal cycle

495 The time sampling is limited for CALIPSO-GOCCP and 2BFLX as they observe each location only two times per day at  
about 1:30 and 13:30 local solar time, and they do not implement diurnal variation correction in their algorithm.  
Nevertheless, diurnal variations of the cloud fraction profiles documented by the CATS/ISS lidar (Noel et al., 2019;  
Chepfer et al., 2019) indicate that the average of the cloud profiles collected at 1:30am and 1:30pm time is similar to the  
average of all the profiles collected along the 24 hours with 1:30pm corresponds to the minimum in cloud profiles along the  
500 day, while 1:30am corresponds to a maximum (Fig. XX7 in Noel et al., 2018). But this statement is valid only between 55°S  
and 55°N.

Figure XX11 shows the diurnal surface LW CRE variation observed at SIRTa in France, together with CALIPSO-GOCCP  
and 2BFLX surface LW CRE estimates. This comparison suggests that the average of the two CALIPSO overpasses each  
day is similar to the ground-based observed daily mean over these two sites.

505 The absence of diurnal cycle correction might not be an important source of error in CALIPSO-GOCCP surface LW CRE  
estimates.

## 7. Evaluation of the new surface LW cloud radiative effect against others satellites products

### 7.1 Comparison along piece of orbits at footprint scale

Aqua (CERES), CloudSat, and CALIPSO, and CERES/Aqua satellites are part of the A-Train constellation (Stephens et al., 2002) and are closely matched in time (<5 min) and hence, as they are part of the A-Train constellation (Stephens et al., 2002), and are Therefore they are collocated by default. Therefore, and so we can neglect compare them directly, in assuming that the atmospheric changes occurring within 5 minutes are negligible, the atmospheric change seen by each satellite overpass, and we plot the surface LW CRE retrievals directly to compare them.

Figure 102 shows a comparison between the surface LW CRE from the three spatial satellite retrievals along four pieces of orbits located over regions with different atmospheres and different surfaces. Figure 102 (top panel) shows the vertical CALIPSO-GOCCP cloud vertical-mask (Guzman et al., 2017), and while Figure 102 bottom line-panel represents the comparison between the surface LW CREs.

Orbit A passes over the East Pacific Ocean and observes a deep convective tower, a mid-level opaque cloud at an altitude of 7 km and a low opaque cloud. The differences in surface LW CRE between the three spatial restitutions do not exceed 5 W m<sup>-2</sup>. Nevertheless, within a small part of the orbit between 11.3°-N and 11.8°-N (Fig. B1) we observe that the CALIPSO-GOCCP retrieval is lower than the other two products, because the lidar does not detect a low cloud below  $Z_{FA}$  that is detected by CloudSat (shown in Fig. B1.b)

Orbit B passes over the West Pacific Ocean and observes variable yet shallow clouds in the boundary layer (< 2 km). The  $CRE_{GOCCP}$  is intermittently larger than the other two products by ~15 W m<sup>-2</sup>. CALIPSO-GOCCP (90 m cross track, 330 m along orbit track) detects shallow clouds in the boundary layer and, during the thickest of these, retrieves a surface LW CRE that is larger than the CERES (CloudSat) retrieval, which is based on a 20 km (5km) footprint and might miss these clouds.

Orbit C passes over ocean stratocumulus regions and observes a low opaque cloud. Between 12°-S and 19°-S, the  $CRE_{GOCCP}$  (almost 60 W m<sup>-2</sup>) is smaller than  $CRE_{2BFLX}$  by ~5 W m<sup>-2</sup> and smaller than  $CRE_{CERES}$  by 15 W m<sup>-2</sup>.

Orbit D passes over Antarctica and observes opaque clouds at high (10 km) and mid-level (4–5 km) altitudes. In the presence of high opaque clouds (between 68°-S and 71°-S or between 73°-S and 77°-S),  $CRE_{GOCCP}$  is lower than  $CRE_{CERES}$  by up to 20 W m<sup>-2</sup> and  $CRE_{2BFLX}$  by up to 40 W m<sup>-2</sup>, but typically compares most favourably with  $CRE_{CERES}$  over the full scene.

These orbits show that by not including CloudSat, CALIPSO-GOCCP surface LW CREs are biased low by typically  $10 \text{ W m}^{-2}$  compared to 2BFLX and  $15 \text{ W m}^{-2}$  compared to CERES-CCCM in regions of deep convection. In stratocumulus, CALIPSO-GOCCP is biased low by typically  $5 \text{ W m}^{-2}$  compared to 2BFLX and  $-15 \text{ W m}^{-2}$  compared to CERES-CCCM.

## 540 | 76.2 Global Statistical ~~comparison with other satellites products~~ at footprint scale over ocean

Figure 143a shows a comparison between the surface LW CRE from CALIPSO-GOCCP observations (90 m cross track, 330 m along orbit track) collocated with CERES-CCCM ~~which that uses full-resolution CALIPSO and CloudSat data and reports the results over 20-km CERES footprints. (20-km footprint) over ocean only during 2008.~~ We consider only the CERES-CCCM footprints where all the CALIPSO-GOCCP profiles falling within this footprint are opaque and where there are more than 40 profiles. To retrieve the surface LW CRE from CALIPSO-GOCCP observations at the CERES-CCCM footprint resolutions, we average all  $Z_{T_{\text{Opaque}}}$  falling within CERES-CCCM's footprint and compute the surface LW CRE using the relationships found in Sect. 4.

We see a strong correlation between the surface LW CRE from CERES-CCCM observations and the surface LW CRE from CALIPSO-GOCCP observations ( $R=0.85$ ). Two significant departures from the one-to-one comparison line are observed: one for high values of the surface LW CRE, and the ~~other second one~~ for low values. In the first pattern, for surface LW CRE greater than  $70 \text{ W m}^{-2}$ ,  $CRE_{GOCCP}$  is larger than  $CRE_{CERES}$ . This pattern corresponds to some low marine opaque clouds in mid-latitude regions (not shown). To reconcile the two products,  $CRE_{GOCCP}$  should be smaller by almost  $5 \text{ W m}^{-2}$ . One way to reduce this difference would be to increase the altitudes of clouds but, due to attenuation of the signal in opaque clouds, the space-based lidar would already potentially overestimate the overall height of the clouds. Thus, the cloud height is likely not the source of this difference. Another way to reduce the surface LW CRE is by decreasing the cloud cover or the cloud opacity. However, ~~thanks to its high spatial resolution,~~ the space-based lidar measures ~~the cloud cover~~ with precision, ~~the cloud cover thanks to its high spatial resolution~~ and it should not overestimate the cloud opacity. Thus, the source of this apparent bias is more likely an underestimation of the humidity profiles used to retrieve the surface LW CRE in the presence of clouds. An increase in the humidity at these times would increase the  $F_{\text{Cloudy-freesky}}^{\text{net}}$  and therefore decrease the surface LW CRE. A final possibility for the difference is that each product has a unique estimate of the cloud cover due to vastly different fields-of-view. CALIOP footprints are only a small fraction of the CERES footprint, so part of the CERES footprint could be cloud free even if the 40 CALIOP profiles are opaque. A study by Kato et al. (2010) demonstrated that the differences between CERES and CloudSat/CALIPSO cloud fractions decrease when averaged over area and time. ~~Hence, so~~ this difference is likely not the primary source of bias when comparing large statistical datasets.

The second regime of differences among the products is for surface LW CRE less than  $30 \text{ W m}^{-2}$  (Fig. 143a), which corresponds to high opaque clouds over the warm pool region (not shown). Here,  $CRE_{GOCCP}$  is smaller than  $CRE_{CERES}$ . The underestimation of surface LW CRE by CALIPSO-GOCCP compared to CERES-CCCM could be caused by the full

attenuation of the laser beam in deep convective clouds such that CALIPSO–GOCCP overestimates the mean altitude of opaque clouds.

570 Figure 143b represents the comparison between the surface LW CRE from CALIPSO–GOCCP observations (90 m cross track, 330 m along orbit track) collocated with CloudSat 2BFLX product at a resolution of CloudSat footprint (5 km). We also consider only the CloudSat footprints where all the CALIPSO–GOCCP profiles falling within this footprint are opaque, and where there are more than 10 profiles, and we compute  $CRE_{GOCCP}$  by averaging all  $Z_{T_{Opaque}}$  falling within CloudSat footprint.

575 Three significant departures from the one-to-one comparison line are observed: one for low values where CALIPSO–GOCCP < 2BFLX, one for high values of the surface LW CRE where CALIPSO–GOCCP > 2BFLX, and one for high values where CALIPSO–GOCCP < 2BFLX. The two first patterns appear to be similar to Fig. 143a, and show up for the same reasons as described above. The last pattern of differences among the products is for large values of CRE where 2BFLX is larger than CALIPSO–GOCCP. This pattern corresponds to a sub-sample of marine opaque clouds (25% of the opaque cloud collocated) in mid-latitude regions (not shown) where CloudSat is able to detect lower clouds than CALIPSO. 580 Using  $Z_{FA}$  instead of  $Z_{T_{Opaque}}$  in CALIPSO–GOCCP retrieval would shift this pattern upward, and reduce the sample (17% Vs 25%).

The differences shown in Fig. 143 are expected when comparing satellite products at footprint scales that use different remote sensing techniques. However, when looking at the gridded product distributions (fig. B43) instead of instantaneous 585 collocated data, the 2BFLX and CALIPSO–GOCCP agree well.

~~6.3 Global mean comparison with other satellites products at gridIn global annual mean, CALIPSO–GOCCP is equal compared to CERES–EBAF (–) and slightly higher compared to 2BFLX (–; 0.7 W m<sup>–2</sup>).~~

~~Compared to CERES–EBAF (Fig. 12a), is larger than over the oceans (except in stratocumulus regions) while is smaller than over icy surfaces and over ocean stratocumulus regions. The larger differences (–14 to –18 W m<sup>–2</sup>) occur over Greenland, Antarctica and tropical stratocumulus regions. Over icy areas like Greenland and the Antarctic ice sheet, CERES–EBAF has limited ability to differentiate the radiative fluxes emitted by the surface from those emitted by the clouds (Liu et al., 2010; Stubenrauch et al., 2013). The retrieval of surface LW CRE with CERES rely on the cloud detection from MODIS–CERES, which detects more clouds than others satellites over icy surfaces (GEWEX Cloud Assessment; Stubenrauch et al., 2012). Similarly, since stratocumulus clouds are low warm clouds at temperatures close to the surface 590 temperature, the CERES radiometer can also have some bias when differentiating the LW cloud fluxes from LW surface fluxes over these regions.~~

~~Compared to 2BFLX (Fig. 12b), is slightly larger than over tropical oceans. Over lands, is slightly lower than . The maximum difference occurs over land along the western coasts of the North and South American continents and the Himalayan mountains where the surface elevation is above 2.5 km. This difference might be due to the CloudSat CPR’s long~~

powerful pulse (Fig. B2), which generates a surface clutter echo that tends to partially mask signals from cloud forming below  $\sim 1$  km (Marchand et al., 2008). Over icy polar areas, the two products are very similar.

6.3. Figure 12c shows the difference between  $\bar{\tau}_{\text{LW}}^{\text{CERES-EBAF}}$  and  $\bar{\tau}_{\text{LW}}^{\text{2BFLX}}$ . The same patterns are observed over continent polar regions as in Fig. 12a, where CERES-EBAF overestimates the surface LW CRE compared to the 2BFLX product.

Zonal averages of the surface LW CRE for 2008–2010 (Figure 12d) show that the surface LW CRE is generally low in tropical regions and increases towards the mid-latitudes as the atmospheric moisture decreases. Values do not vary by much northward of about  $50^\circ$  N. To the south, a maximum occurs at about  $60^\circ$  S, with a decline towards the far south due to declines in cloudiness. Over the broad domain reaching from  $60^\circ$  N to  $60^\circ$  S the three satellites techniques show similar zonal means with differences among the three typically not exceeding  $3 \text{ W m}^{-2}$ . Over polar regions, the surface LW CRE from CERES-EBAF is generally higher than the other two products derived from active sensors.

#### 6.4 Comparison with ground-based stations at gridded scale

Comparisons between ground-based measurements and the satellite-derived products ( $\bar{\tau}_{\text{LW}}^{\text{CALIPSO-GOCCP}}$ ,  $\bar{\tau}_{\text{LW}}^{\text{2BFLX}}$ ,  $\bar{\tau}_{\text{LW}}^{\text{CERES-EBAF}}$ ) provide a direct evaluation of the satellite retrievals, but are limited by the difference in the spatial resolution of the satellite-derived product ( $2^\circ \times 2^\circ$ ) and the ground station observations (a few meters). The locations of the three ground-based sites are reported in the maps (stars in Fig. 12e).

Over the Summit Station, Greenland site, on average compared to ground-based observations, CALIPSO-GOCCP underestimates the surface LW CRE by  $8.5 \text{ W m}^{-2}$ , while 2BFLX underestimates it by  $16.4 \text{ W m}^{-2}$  and CERES-EBAF overestimates it by  $36.6 \text{ W m}^{-2}$  (Fig. 13a). The comparison of averages is made only when all products are available and for the Greenland site, this is just for three months (JFM 2011). Averages over the 2008–2011 and 2011–2016 periods (Fig. 14) show that these biases calculated for a short period are similar to the longer periods. Over the 2008–2011 time period,  $\bar{\tau}_{\text{LW}}^{\text{CALIPSO-GOCCP}}$  is close to  $\bar{\tau}_{\text{LW}}^{\text{ground}}$  and both show consistent summer maxima and winter minima.  $\bar{\tau}_{\text{LW}}^{\text{2BFLX}}$  follows a different annual cycle with maxima wider and shifted by about two to six months. Over the 2011–2016 time period,  $\bar{\tau}_{\text{LW}}^{\text{CALIPSO-GOCCP}}$  and the ground station data show similar annual cycles, while the annual cycle continues to be shifted by two to four month and generally has different annual variability compared to ground station. The same behavior where CERES-EBAF overestimates the surface LW CRE comparing to CALIPSO-GOCCP is observed over the map of difference (Fig. 12a) in icy polar regions, for instance over Greenland and Antarctica ice sheet. While this comparison suggests that CALIPSO-GOCCP could be biased some compared to the ground-station perspective over Greenland, it is also clear that this approach does appropriately capture the annual variability, while the CERES-EBAF approach appears to be significantly biased high with an unrealistic annual cycle.

Over the mid-latitude continental site (Fig. 13b) on average, CALIPSO-GOCCP underestimates the surface LW CRE by  $5.7 \text{ W m}^{-2}$  compared to ground-based observations, while 2BFLX underestimates it by  $9.4 \text{ W m}^{-2}$  and CERES-EBAF underestimates it by  $12.1 \text{ W m}^{-2}$ .

Over the tropical ocean site (Fig. 13c) on average, CALIPSO-GOCCP underestimates the surface LW CRE by  $2.3 \text{ W m}^{-2}$  compared to ground-based observations, while CERES-EBAF underestimates it by  $2.7 \text{ W m}^{-2}$  and 2BFLX underestimates it by  $4.1 \text{ W m}^{-2}$ . This same behavior is found on the map of differences between  $\bar{\tau}_{\text{LW}}^{\text{CALIPSO-GOCCP}}$  and  $\bar{\tau}_{\text{LW}}^{\text{ground}}$  (Fig. 12b) along the tropical Pacific and

635

tropical Atlantic oceans where 2BFLX underestimates the surface LW CRE comparing to CALIPSO-GOCCP. 7.1.1 Over ground-base sites

640

Figure 14 presents the comparison of seasonal cycles between the satellite retrievals and the ground-based observations. Over the Greenland site (Fig. 14a,d), CALIPSO-GOCCP and 2BFLX find the same seasonal cycle of the surface LW CRE with maxima in July, that correspond to the maximum opaque cloud cover, same as the ground-based seasonal cycle. The CERES-EBAF retrieval maximum is shifted by about three months (October, Fig. 14a,d), to a time of year that shows the minimum opaque cloud cover based on CALIPSO-GOCCP (not shown). This result suggests that during these months the CERES-EBAF retrieval does not successfully distinguish LW upward fluxes from clouds and the surface. This is consistent with CERES-EBAF low-mid and high-mid cloud fractions being biased high over the Summit site except for summer time (not shown). Consistently, Figure 14d shows CERES-EBAF's surface LW CRE is overestimated compared to ground-base retrievals in all season except summer. As a consequence CERES-EBAF does not capture the surface LW CRE annual cycle, contrarily to CALIPSO-GOCCP and 2BFLX retrievals.

645

Over the mid-latitude continental site (Fig. 14b,e), the surface LW CRE seasonal cycle of CALIPSO-GOCCP and 2BFLX are close to each other and the three satellite-derived products show similar seasonal cycles as the ground station. Over the tropical-ocean site (Fig. 14c,f), the surface LW CRE seasonal cycle is relatively flat.

~~CALIPSO does not see the cloud base in many stratiform-type clouds, as an example, but this does not lead to as big of an issue in the surface LW CRE retrieval because the stratiform cloud base is not very far from the point of attenuation of the lidar. On the other hand, this attenuation can become a significant issue for circumstances where the lidar signal is fully attenuated at an altitude that is significantly above the actual cloud base, such as in deep convective clouds.~~

~~Based on the comparison of orbits (Fig. B1), we observe that when the space lidar does not see the cloud base, CALIPSO LW CRE underestimates the local surface LW CRE compared to 2BFLX. However, the opaque deep convective clouds cover a small part of the overall tropics compared to other clouds, therefore this effect does not dominate the global comparison (Fig. 12) where CALIPSO GOCPP surface LW CRE, is on the contrary, slightly larger than the other satellite products.~~

~~To test if the differences between CALIPSO GOCPP and other products come from the space lidar not seeing the cloud base, we used  $\tau_{\text{cloud}}^{\text{lidar}}$  instead of  $\tau_{\text{cloud}}^{\text{surface}}$  in the CALIPSO GOCPP retrieval. By definition  $\tau_{\text{cloud}}^{\text{lidar}}$  is always lower in altitude than  $\tau_{\text{cloud}}^{\text{surface}}$ , therefore this change should reduce the difference between the CALIPSO GOCPP surface LW CRE and other surface LW CREs if the differences were due to CALIPSO missing the cloud base. Fig. B3 shows that the difference between CALIPSO GOCPP surface LW CRE and the other satellite products increases instead of reduces when using  $\tau_{\text{cloud}}^{\text{lidar}}$  instead of  $\tau_{\text{cloud}}^{\text{surface}}$ . This suggests that the differences in surface LW CRE are likely not often due to CALIPSO misrepresenting the cloud base and that the cloud base might not be far from in the majority of the cases. This result also suggests that the differences between the satellite retrievals come from other sources, such as the assumed humidity and temperature profiles. Indeed, the resolution of these profiles is rough in the CALIPSO retrieval and these profiles have also been identified as the largest sources of LW flux uncertainty in the 2BFLX product (Henderson et al., 2013).~~

~~Nevertheless contrarily to the satellite retrieval inter-comparison, using  $\tau_{\text{cloud}}^{\text{lidar}}$  instead of  $\tau_{\text{cloud}}^{\text{surface}}$  leads to slightly better agreement of CALIPSO GOCPP LW CRE with ground-based retrievals (eg. Fig. 13, 14). Ground-based measurements derive directly the surface LW CRE. While there are certainly challenges in comparing ground-based and satellite estimates, we should consider the ground-based estimates to be of pretty high quality. Thus, what these results mean collectively is that: 1) The inability of CALIPSO to observe the cloud base likely does have some effect (with respect to ground-based measurements). And that 2) this effect actually makes the comparison with other satellite products worse, which means that there are other issues (possibly with the other satellite products) leading to further difference,,,,,~~

2BFLX is a  $1^\circ \times 1^\circ$  gridded product and CALIPSO-GOCCP is a  $2^\circ \times 2^\circ$  gridded product. To compare the two product, 2BFLX and CALIPSO-GOCCP at gridded scale, we is-averaged 2BFLX initially at  $1^\circ \times 1^\circ$  resolution to  $2^\circ \times 2^\circ$  like CALIPSO-GOCCP, over  $2^\circ \times 2^\circ$  then subtracted from CALIPSO-GOCCP.

685 | -Figure 124a shows global maps of differences between CALIPSO-GOCCP and the other satellite-derived products (CERES-EBAF and 2BFLX). This comparison gives an overview of the differences between the threetwo surface LW CRE spatial products, but it may mask some differences given the fact that the three-two spatial products are averaged in time (monthly) and space ( $2^\circ \times 2^\circ$  latitude-longitude gridded).

In global annual mean, CALIPSO-GOCCP is-equal-compared-to CERES-EBAF () and slightly higher compared to 2BFLX ( $CRE_{2BFLX}$ ;  $0.7 \text{ W m}^{-2}$ ).

690 | ompared to CERES-EBAF (Fig. 12a), is larger than over the oceans (except in stratocumulus regions) while is smaller than over icy surfaces and over ocean stratocumulus regions. The larger differences ( $-14$  to  $-18 \text{ W m}^{-2}$ ) occur over Greenland, Antarctica and tropical stratocumulus regions. Over icy areas like Greenland and the Antarctic ice sheet, CERES-EBAF has limited ability to differentiate the radiative fluxes emitted by the surface from those emitted by the clouds (Liu et al., 2010; Stubenrauch et al., 2013). The retrieval of surface LW CRE with CERES rely on the cloud detection from MODIS-CERES, which detects more clouds than others satellites over icy surfaces (GEWEX Cloud Assessment; Stubenrauch et al., 2012). Similarly, since stratocumulus clouds are low warm clouds at temperatures close to the surface temperature, the CERES radiometer can also have some bias when differentiating the LW cloud fluxes from LW surface fluxes over these regions.

700 | Compared to 2BFLX (Fig. 12b),  $CRE_{GOCCP}$  is slightly larger than  $CRE_{2BFLX}$  over tropical oceans. Over lands,  $CRE_{GOCCP}$  is slightly lower than  $CRE_{2BFLX}$ . The maximum difference occurs over land along the western coasts of the North and South American continents and the Himalayan mountains, where the surface elevation is above 2.5 km. This difference might be due to the CloudSat CPR's long powerful pulse (Fig. B2), which generates a surface clutter echo that tends to partially mask signals from clouds forming below  $\sim 1 \text{ km}$  (Marchand et al., 2008). Over icy polar areas, the two products are very similar.

705 | Figure 12c shows the difference between and -. The same patterns are observed over continent polar regions as in Fig. 12a, where CERES-EBAF overestimates the surface LW CRE compared to the 2BFLX product.

Zonal averages of the surface LW CRE for 2008–2010 (Figure 12d4c) show that the surface LW CRE is generally low in tropical regions and increases towards the mid-latitudes as the atmospheric moisture decreases. Values do not vary by much northward of about  $50^\circ\text{-N}$ . To the south, a maximum occurs at about  $60^\circ\text{-S}$ , with a decline towards the far south due to lessdeclines-in cloudiness. Over the broad domain, reaching from  $60^\circ\text{-N}$  to  $60^\circ\text{-S}$ , the threetwo satellites techniques show



similar zonal means, with differences among the ~~three~~<sup>two</sup> typically not exceeding  $3 \text{ W m}^{-2}$ . ~~Over polar regions, the surface LW CRE from CERES-EBAF is generally higher than the other two products derived from active sensors.~~

## 7.1 Seasonal variation

### 715 7.1.1 Over-ground base sites

Figure 14 presents the comparison of seasonal cycles between the satellite retrievals and the ground-based observations.

Over the Greenland site (Fig. 14a,d), CALIPSO-GOCCP and 2BFLX find the same seasonal cycle of the surface LW CRE with maxima in July, that correspond to the maximum opaque cloud cover, same as the ground-based seasonal cycle. The CERES-EBAF retrieval maximum is shifted by about three months (October, Fig. 14a,d), to a time of year that shows the  
720 minimum opaque cloud cover based on CALIPSO-GOCCP (not shown). This result suggests that during these months the CERES-EBAF retrieval does not successfully distinguish LW upward fluxes from clouds and the surface. This is consistent with CERES-EBAF low-mid and high-mid cloud fractions being biased high over the Summit site except for summer time (not shown). Consistently, Figure 14d shows CERES-EBAF's surface LW CRE is overestimated compared to ground-base retrievals in all season except summer. As a consequence CERES-EBAF does not capture the surface LW CRE annual  
725 cycle, contrarily to CALIPSO-GOCCP and 2BFLX retrievals.

Over the mid-latitude continental site (Fig. 14b,e), the surface LW CRE seasonal cycle of CALIPSO-GOCCP and 2BFLX are close to each other and the three satellite-derived products show similar seasonal cycles as the ground station.

6. Over the tropical ocean site (Fig. 14c,f), the surface LW CRE seasonal cycle is relatively flat.

#### 7.1.2 Global mean (2008–2020)

730 Figure 15a represents the global average seasonal cycle of the three surface LW CRE satellite-derived products. It is larger than and from October to February and is lower from May to September. To analyze these differences, we decomposed the globe into Northern Hemisphere (NH : Fig. 15b), NH-ocean (Fig. 15c), NH-land (Fig. 15d), and Southern Hemisphere (SH : Fig. 15e), SH-ocean (Fig. 15f), SH-land (Fig. 15g).

735 The NH winter is the main cause for CERES-EBAF being larger than the two other products from October to February ( $2-3 \text{ W m}^{-2}$ ). The NH continents have the largest contribution ( $\sim 6 \text{ W m}^{-2}$ ) and the NH-oceans contribute slightly ( $\sim 1 \text{ W m}^{-2}$ ) between January to March which corresponds to the maximum of sea ice (Rousset et al., 2015). The SH only contributes a little ( $\sim 0.5 \text{ W m}^{-2}$ ) for the months of October and November and this comes only from the Antarctic ice sheet, which is covered by ice all year long. Same as in the difference maps (Fig. 12a), MODIS-CERES detects more clouds than other satellites over icy surfaces (GEWEX Cloud Assessment ; Stubenrauch et al., 2012).

740 The lower CERES-EBAF compared to CALIPSO-GOCCP and 2BFLX ( $1-2 \text{ W m}^{-2}$ ) from May to September is mostly caused by both the oceans in SH and the land in NH.

#### 7.1.3 Seasonal evolution of the zonal mean

745 Figure 16 represents the annual evolution of the zonal mean of the surface LW CRE from CERES-EBAF (Fig. 16a), CALIPSO-GOCCP (Fig. 16b), and 2BFLX (Fig. 16c). The two active sensor figures exhibit the same behavior whilst CERES-EBAF has a stronger surface LW CRE in the polar regions during winter months, which corresponds to the minimum of opaque cloud cover and the maximum of sea ice. To see where the largest differences with CERES-EBAF are located, Figures 16d and 16e represent the differences between CALIPSO-GOCCP and CERES-EBAF and the differences between 2BFLX and CERES-EBAF respectively. The same feature is observed in both figures with CERES-EBAF having larger surface LW CRE than the other two products in the polar regions during their respective winters. CERES-EBAF also has smaller surface LW CRE in the mid-latitude regions.

750 Decomposing the difference (Fig. 16d) into land only (Fig. 16f) and ocean only (Fig. 16g) shows CALIPSO-GOCCP lower than CERES-EBAF over NH land [ $50^\circ \text{ N}$  to  $80^\circ \text{ N}$ ] during winter (September to May) and over the icy Antarctic all year long. The oceans contribute to this difference during months of significant sea ice. These results suggest that the differences in surface LW CRE are likely due to CERES-EBAF detecting clouds over icy surfaces when there are no clouds (Stubenrauch et al., 2012).

760 On the contrary, CERES-EBAF is lower than CALIPSO-GOCCP mostly over mid-latitude oceanic regions all year long (Fig. 16g) and this difference is also observed in the annual mean maps (Fig. 12a). These regions contain low altitude thin clouds and few low opaque clouds ( $1-2 \text{ km}$ : Fig. 2b,d). To see if these differences are caused by thin clouds in the boundary layer, we have computed the difference between the surface LW opaque CRE from CALIPSO-GOCCP observations and the CERES-EBAF product (Fig. 16h) over ocean only. The differences over mid-latitude oceans are smaller and close to 0 in this case (Fig. 16h). Thus, the reason for the CERES-EBAF surface LW CRE being weaker than the CALIPSO-GOCCP in these regions is likely because the CERES radiometer does not see the optically thin clouds in the boundary layer over mid-latitude oceans.

#### 7.4.2 Variations of 13 years (2008–2020)

765 | Figure 175a shows the temporal evolution of the surface LW CRE anomaly from the ~~threetwo~~ satellite-derived ~~products~~. ~~products over 13 years 2008–202~~. A decomposition, separating continents from oceans and NH from SH, is presented in Figs. 17b–g.

There is a consistent amplitude in the annual variability in the global surface LW CRE anomaly between the three datasets. This appears to be because of the annual cycle variations in the SH and NH, which are out of sync from with respect to each other, and the fact that the SH annual amplitude (and magnitude) are larger. Thus, the annual variation of the global surface LW CRE is most closely aligned with the annual variation of the SH.

770 | The phasing of the annual cycle of  $CRE_{GOCCP}$  and  $CRE_{2BFLX}$  anomalies are roughly similar over the 2008–2010 time period, while, as noted before but for a specific location, the anomaly shows a shift in the annual cycle of about two months compared to the other two satellite-derived products. This shift remains between and anomalies over the 13 years. **The phasing of the annual cycle for the CERES-EBAF of the two products is actually quite consistent with the others for both NH and SH over both land and ocean, except for the NH land (Fig. 17d; because of false cloud detection as already explained and shown in Figs. 14–16), the  $CRE_{2BFLX}$  is slightly larger than  $CRE_{GOCCP}$ . However, it is interesting that even over NH land the annual minima match pretty well.** Thus, the overall two months shift (Fig. 17a) is in part due to the differences in NH land annual maximum but apparently also somewhat due to the different amplitudes of the annual cycles for different areas and how they combine in unique ways for the different datasets.

780 | The inter-annual variability is pretty interesting. For example, the NH winter maximum in CERES-EBAF and CALIPSO-GOCCP products appears to vary by up to about  $3 \text{ W m}^{-2}$  from year to year. That is the kind of variability that might have significant impacts on climate-relevant processes like melting of the cryosphere.

785 |

## 8. Discussion

### 8.1 About the space lidar missing the opaque cloud base

CALIPSO does not see the cloud base in many stratiform-type clouds, as an example, but this does not lead to as big of an issue in the surface LW CRE retrieval because the stratiform cloud base is not very far from the point of attenuation of the lidar. On the other hand, this attenuation can become a significant issue for circumstances where the lidar signal is fully attenuated at an altitude that is significantly above the actual cloud base, such as in deep convective clouds.

Based on the comparison of orbits (Fig. B1), we observe that when the space lidar does not see the cloud base, CALIPSO-GOCCP surface LW CRE underestimates the local surface LW CRE compared to 2BFLX. However, the opaque-deep convective opaque clouds cover a small part of the overall tropics compared to other clouds. Therefore, this effect does not dominate the global comparison (Fig. 14a), where CALIPSO-GOCCP surface LW CRE is on the contrary, slightly larger than the other satellite product. Figure 13b (where 2BFLX is about  $70 \text{ W/m}^2$ ) and Figure 14a (Southern Ocean) consistently suggest that CALIPSO not seeing cloud base leads to CALIPSO-GOCCP underestimating the surface LW CRE more frequently in the extra-tropical oceanic storm tracks than elsewhere.

To test if the differences between CALIPSO-GOCCP and other satellite products come from the space lidar not seeing the cloud base, we used two different approaches.

First, we used  $Z_{FA}$  instead of  $Z_{T_{Opaque}}$  in the CALIPSO-GOCCP retrieval. By definition  $Z_{FA}$  is always lower in altitude than  $Z_{T_{Opaque}}$ . Therefore, this change should reduce the difference between the CALIPSO-GOCCP surface LW CRE and other surface LW CREs, if the differences were due to CALIPSO missing the cloud base. Fig. 14b shows that the difference between CALIPSO-GOCCP surface LW CRE and the other satellite products increases instead of reduces when using  $Z_{FA}$  instead of  $Z_{T_{Opaque}}$ . This suggests that the differences in surface LW CRE are likely not often due to CALIPSO misrepresenting the cloud base and that, in the majority of the cases, the cloud base might not be far from  $Z_{FA}$  in the majority of the cases. Nevertheless, contrarily to the satellite retrieval inter-comparison, using  $Z_{FA}$  instead of  $Z_{T_{Opaque}}$  leads to slightly better agreement between CALIPSO-GOCCP LW CRE with ground-based retrievals (e.g., Fig. 9, 10). Ground-based measurements derive directly the surface LW CRE. While there are certainly challenges in comparing ground-based and satellite estimates, we should consider the ground-based estimates to be of pretty high quality.

Second, we used the cloud-base height (called CBASE dataset) described in Mülmenstädt et al. (2018) instead of  $Z_{FA}$  to compute  $Z_{T_{Opaque}}$ . In the CBASE dataset, the Cloud base-height value is given at a horizontal resolution of 40 km along the CALIPSO orbit track in the portion of the orbit where clouds are opaque. Along each CALIPSO orbit, we collocated the cloud-base height dataset with the CALIPSO-GOCCP dataset and replaced  $Z_{FA}$  by the Cloud-base-height value given in the CBASE dataset. Then we computed  $Z_{T_{Opaque}}$  and the Surface LW CRE. CBASE values are distributed in all latitudes and are available in 33.2% of all the CALIPSO opaque profiles because CBASE can be retrieved only when thin clouds are detected within the 40 km orbit piece that also contains opaque clouds profiles. Comparing Fig. 16a and b indicates that the subsample of opaque CALIPSO-GOCCP profiles where CBASE is documented contains both large values of surface LW CRE associated to mid- and low-level clouds located at mid-latitudes (upper right data in plot b) and small values of CRE (lower left), but it does not include the data where 2BFLX is much larger than CALIPSO-GOCCP which correspond to mid-latitude oceanic opaque clouds. When replacing  $Z_{FA}$  (Fig. 16be) by CBASE (Fig. 16cb) in the CALIPSO-GOCCP algorithm, the CRE CALIPSO-GOCCP rises up slightly almost everywhere because CBASE is lower in altitude than  $Z_{FA}$ , and CALIPSO-GOCCP CRE values lower than  $18 \text{ W m}^{-2}$  are no more present. These latter correspond to both deep convective clouds and shallow boundary layer clouds. The correlation between 2BFLX and CALIPSO-GOCCP is similar whether we use  $Z_{FA}$  (0.79) or CBASE (0.78) in the CALIPSO-GOCCP algorithm.

This sensitivity study suggests that using a more advanced cloud base height (here CBASE) than  $Z_{FA}$  derived from lidar measurements than  $Z_{FA}$ , i.e.,  $Z_{FA}$  in CALIPSO-GOCCP algorithm will increase slightly the CRE value retrieved in some opaque cloud profiles slightly, but it does not fundamentally change the results.

Thus, what these results mean collectively is that: 1) The inability of CALIPSO to observe the cloud base likely does have some effect (with respect to ground-based measurements). And that 2) This effect actually makes the comparison with other satellite products worse, which means that there are other issues (possibly also with the other satellite product) leading to further differences

## 8.2 About the sub-daily variability of the Humidity and temperature profiles

Looking for other issues that could explain the differences between satellite products, we examined humidity and temperature profiles.

Contrarily to the CALIPSO-GOCCP surface LW CRE retrieval method, CERES-CCCM and 2BFLX retrievals of surface flux account for sub-daily variations in temperature/humidity and capture regional variations (e.g., eastern -vs. western tropical

Pacific), climate events (e.g., ENSO) and extreme changes over polar regions. – 2BFLX uses 3-hourly atmospheric state variable data on a half-degree Cartesian latitude and longitude grid from AN-ECMWF.

845 As shown in Fig. 14, monthly mean gridded surface LW CRE from CALIPSO-GOCCP are consistent with 2BFLX, even though 2BFLX uses sub-daily spatio-temporal resolutions of temperature/humidity profiles, while CALIPSO-GOCCP uses monthly means temperature/humidity profiles. Nevertheless, instantaneous CALIPSO-GOCCP surface LW CRE retrieval are likely more biased than the monthly mean gridded CALIPSO-GOCCP surface LW CRE, due to the use of monthly means temperature/humidity profiles, because monthly means miss extremes humidity and temperature profiles. To estimate the error on the instantaneous GOCCP surface LW CRE values, we compared the instantaneous CALIPSO-GOCCP values obtained using 6-hourly daily temperature/humidity profiles from ERAi, with the one obtained using monthly means and with 2BFLX, for one day at footprint scales.

850

Figure XX-17 shows that using sub-daily profiles in CALIPSO-GOCCP makes the comparison with other satellite products worse at footprint scale. – More analysis (not shown) indicate that for thin clouds, CALIPSO-GOCCP surface LW CRE retrieved using sub-daily temperature-/humidity profiles agrees better with 2BFLX (at 5km resolution) than CALIPSO-GOCCP surface LW CRE retrieved using monthly mean profiles. In contrast, the agreement between CALIPSO-GOCCP and others products are lower when using sub-daily temperature-/humidity profiles in all other cases: opaque clouds and also thin clouds when compared to CERES-CCCM (2at 20km). Overall, this suggests that the differences between the three gridded daily products are likely due to others causes than CALIPSO-GOCCP using monthly mean temperature-/humidity profiles.

855

860

## 9 Conclusion

In this paper, we build a new surface LW CRE dataset from five cloud properties observed with space-based lidar (CALIPSO–GOCCP). The robustness of the new surface LW CRE dataset at global scales is evaluated by comparing it ~~against-to~~ existing independent space-based surface LW CRE retrievals from CERES and CloudSat (Kato et al., 2010; L’Ecuyer et al., 2019) at ~~footprint~~ instantaneous ~~footprint~~ scale, as well as at  $2^\circ \times 2^\circ$  gridded ~~global~~ scale ~~globally~~. It is also evaluated locally by comparison ~~against-with~~ observations collected at three ground stations in polar (Shupe et al., 2013), mid-latitude (Haeffelin et al., 2005; Chiriaco et al., 2018) and tropical (Roesch et al., 2011) locations. The (admittedly limited) ground-station comparisons actually showed that the CALIPSO–GOCCP product agreed the best with the ground measurements compared to the other satellite products, ~~especially-in~~. ~~It appears that it captures-well~~ the ~~inter-annual~~ variability ~~well~~. Additionally, there are other specific aspects where the CALIPSO–GOCCP product appears to be an improvement over others, ~~in providing a longer time series~~, **including over bright polar surfaces**.

This might be surprising given the simplicity of the surface radiation retrieval method used to produce the CALIPSO–GOCCP product, but ~~it-this~~ is understandable because of the two following physical elements:

i) The CALIPSO–GOCCP method directly retrieves the surface LW CRE without retrieving the surface radiative fluxes first. This approach minimizes the impact of the uncertainties due to surface characteristics (surface emissivity, roughness, deserts and frozen surfaces), which strongly influence the fluxes but not the surface LW CRE.

ii) The surface LW CRE is primarily driven by the cloud cover, the cloud opacity and the cloud altitude, which are ~~quite-well measured~~~~documented~~ by space-based lidar over all types of surfaces. Moreover, the lidar approach distinguishes quite well the opaque clouds from the optically thin clouds. Lastly, it documents the detailed vertical cloud profile, except below the altitude where the laser is fully attenuated where we overestimate the mean altitude of opaque clouds. This last limitation only weakly influences the surface LW CRE retrieval because the lidar is fully attenuated at an altitude lower than 3 km above the surface most of the time (Guzman et al., 2017), except in deep convection and some mid-latitude clouds. Indeed, along deep convective tropical regions where the attenuation of the lidar beam might not see the whole bottom part of the cloud and can underestimate the surface LW CRE by almost  $5 \text{ W m}^{-2}$ . All three satellite datasets exhibit some differences relative to ground-based measurements.

The evaluation of this new CALIPSO–based surface LW CRE against other datasets also showed that (overall) this new retrieval agrees well with CloudSat-based estimates (L’Ecuyer et al., 2019) ~~and CERES-CCCM~~, but ~~these~~ ~~latters~~ ~~is~~~~are~~ limited in time until only 2011 due to a battery anomaly. ~~Compared to CERES-EBAF, the new CALIPSO–GOCCP-based dataset provides new and more reliable information on the surface LW CRE over specific regions such as over icy and~~

continental regions, where space-based lidar is successful in distinguishing clouds from the surface, and over mid-latitude oceans, where space-lidar detects well optically thin small clouds well

This new global dataset extends over more than a decade, thanks to the long CALIPSO mission. The global mean temporal evolution over 13 years (2008–2020) shows that the maximum anomaly of the surface LW CRE derived from CALIPSO–GOCCP in the NH winter varies by up to about  $3 \text{ W m}^{-2}$  from year to year, is shifted by about two months compared to that derived from the passive CERES radiometer. This shift is mostly due to differences over the NH lands during winter when the surface is icy. This new dataset will be extended in time by including future data acquired by CALIPSO, as well as with data collected by forthcoming space lidars on-board the European Earth Cloud, Aerosol and Radiation Explorer mission (EarthCARE; Illingworth et al., 2015) and the next generation of US cloud/aerosols lidar space missions if we are able to reconcile data from successive space lidar missions.

The dataset presented in this paper will be used in a future study to better understand the mechanisms of cloud radiative feedbacks at the Earth's surface, i.e. how a change in surface temperature modifies the cloud properties that change the surface LW CRE, which in turn influences the temperature. An essential first step is to understand which cloud variables have driven the surface LW CRE variations over the last decade in regions that are most sensitive to global warming, such as the polar regions, as well as on a global scale. Several recent studies (e.g., Taylor et al., 2007; Zelinka et al., 2012a, 2012b; Vaillant de Guélis et al., 2017a, 2017b, 2018) have shown that it is possible to attribute changes in CRE to variations in cloud properties when 1) the CRE is related to a limited number of cloud properties by sufficiently simple relationships that they can be derived analytically, 2) the CRE retrieved by these analytical relationships is sufficiently reliable, i.e. within the uncertainty domain of the existing datasets, and 3) the CRE is retrieved using reliable observations over all surface types and on long global time scale. The CALIPSO–GOCCP surface LW CRE dataset developed in this study satisfies these three conditions. The next step of this work will therefore be to analyze this 13-years dataset to understand these mechanisms. The goal of this research is to improve our understanding of the response of clouds to the warming induced by anthropogenic activities, which is a major source of uncertainty in climate change predictions.

*Acknowledgements.* We are grateful to Airbus for contributing to the funding of the PhD grant of the first author. We acknowledge Jean Lac for technique support and Erik Hojgard-Olsen for editing the texte. We acknowledge NASA/CNES for the CALIPSO–level–1 data and the Mesocentre ESPRI/IPSL for the computational resources. We recognize the support of CNES who supported the development of the CALIPSO–GOCCP product. MDS and MRG acknowledge support from the National Science Foundation grants PLR-1314156 and OPP-1801477.



*Data:* the new CALIPSO–GOCCP surface LW CRE dataset presented in this paper will be made available on <https://climserv.ipsl.polytechnique.fr/cfmip-obs/index.html>

#### **Appendix A: Sensitivity of the surface LW CRE to humidity and temperature**

#### **930 Appendix B: Sensitivity of the surface LW CRE to cloud base height**

## References

- Acquaotta, F. and Fratianni, S.: THE IMPORTANCE OF THE QUALITY AND RELIABILITY OF THE HISTORICAL TIME SERIES FOR THE STUDY OF CLIMATE CHANGE, *ABClimate*, 14, <https://doi.org/10.5380/abclimate.v14i1.38168>, 2014.
- 935 Allan, R. P.: Combining satellite data and models to estimate cloud radiative effect at the surface and in the atmosphere: Cloud radiative effect at the surface and in the atmosphere, *Met. Apps*, 18, 324–333, <https://doi.org/10.1002/met.285>, 2011.
- van den Broeke, M., Bamber, J., Ettema, J., Rignot, E., Schrama, E., van de Berg, W. J., van Meijgaard, E., Velicogna, I., and Wouters, B.: Partitioning Recent Greenland Mass Loss, *Science*, 326, 984–986, <https://doi.org/10.1126/science.1178176>, 2009.
- 940 [Austin, R. T., A. J. Heymsfield, and G. L. Stephens \(2009\). Retrieval of ice cloud microphysical parameters using the CloudSat millimeter-wave radar and temperature, \*J. Geophys. Res.\*, 114, D00A23, doi:10.1029/2008JD010049.](#)
- Cesana, G., Kay, J. E., Chepfer, H., English, J. M., and Boer, G.: Ubiquitous low level liquid containing Arctic clouds: New observations and climate model constraints from CALIPSO GOCCP, *Geophys. Res. Lett.*, 39, 2012GL053385, <https://doi.org/10.1029/2012GL053385>, 2012.
- 945 Chepfer, H., Bony, S., Winker, D., Cesana, G., Dufresne, J. L., Minnis, P., Stubenrauch, C. J., and Zeng, S.: The GCM-Oriented CALIPSO Cloud Product (CALIPSO–GOCCP), *J. Geophys. Res.*, 115, D00H16, <https://doi.org/10.1029/2009JD012251>, 2010.
- Chepfer, H., Brogniez, H., and Noel, V.: Diurnal variations of cloud and relative humidity profiles across the tropics, *Sci Rep*, 9, 16045, <https://doi.org/10.1038/s41598-019-52437-6>, 2019.
- 950 Chiriaco, M., Dupont, J.-C., Bastin, S., Badosa, J., Lopez, J., Haeffelin, M., Chepfer, H., and Guzman, R.: ReOBS: a new approach to synthesize long-term multi-variable dataset and application to the SIRTAs supersite, *Earth Syst. Sci. Data*, 10, 919–940, <https://doi.org/10.5194/essd-10-919-2018>, 2018.
- Chylek, P., Lohmann, U., Dubey, M., Mishchenko, M., Kahn, R., and Ohmura, A.: Limits on climate sensitivity derived from recent satellite and surface observations, *J. Geophys. Res.*, 112, D24S04, <https://doi.org/10.1029/2007JD008740>, 2007.
- 955 [Corti, T. and Peter, T.: A simple model for cloud radiative forcing, 8, 2009.](#)
- Curry, J. A., Schramm, J. L., Rossow, W. B., and Randall, D.: Overview of Arctic cloud and radiation characteristics, 9, 1731–1764, 1996.
- Dee, D. P., Uppala, S. M., Simmons, A. J., Berrisford, P., Poli, P., Kobayashi, S., Andrae, U., Balmaseda, M. A., Balsamo, G., Bauer, P., Bechtold, P., Beljaars, A. C. M., van de Berg, L., Bidlot, J., Bormann, N., Delsol, C., Dragani, R., Fuentes, M.,
- 960 Geer, A. J., Haimberger, L., Healy, S. B., Hersbach, H., Hólm, E. V., Isaksen, L., Kållberg, P., Köhler, M., Matricardi, M., McNally, A. P., Monge-Sanz, B. M., Morcrette, J.-J., Park, B.-K., Peubey, C., de Rosnay, P., Tavolato, C., Thépaut, J.-N., and Vitart, F.: The ERA-Interim reanalysis: configuration and performance of the data assimilation system, *Q.J.R. Meteorol. Soc.*, 137, 553–597, <https://doi.org/10.1002/qj.828>, 2011.
- Driemel, A., Augustine, J., Behrens, K., Colle, S., Cox, C., Cuevas-Agulló, E., Denn, F. M., Duprat, T., Fukuda, M., Grobe, H., Haeffelin, M., Hodges, G., Hyett, N., Ijima, O., Kallis, A., Knap, W., Kustov, V., Long, C. N., Longenecker, D., Lupi,

- A., Maturilli, M., Mimouni, M., Ntsangwane, L., Ogihara, H., Olano, X., Olefs, M., Omori, M., Passamani, L., Pereira, E. B., Schmithüsen, H., Schumacher, S., Sieger, R., Tamlyn, J., Vogt, R., Vuilleumier, L., Xia, X., Ohmura, A., and König-Langlo, G.: Baseline Surface Radiation Network (BSRN): structure and data description (1992–2017), *Earth Syst. Sci. Data*, 10, 1491–1501, <https://doi.org/10.5194/essd-10-1491-2018>, 2018.
- 970 Dubuisson, P.: Water vapor retrieval over ocean using near-infrared radiometry, *J. Geophys. Res.*, 109, D19106, <https://doi.org/10.1029/2004JD004516>, 2004.
- Dupont, J.-C. and Haeffelin, M.: Observed instantaneous cirrus radiative effect on surface-level shortwave and longwave irradiances, *J. Geophys. Res.*, 113, D21202, <https://doi.org/10.1029/2008JD009838>, 2008.
- Gallagher, M. R., Shupe, M. D., and Miller, N. B.: Impact of Atmospheric Circulation on Temperature, Clouds, and  
975 Radiation at Summit Station, Greenland, with Self-Organizing Maps, *J. Climate*, 31, 8895–8915, <https://doi.org/10.1175/JCLI-D-17-0893.1>, 2018.
- Garnier, A., Pelon, J., Vaughan, M. A., Winker, D. M., Trepte, C. R., and Dubuisson, P.: Lidar multiple scattering factors inferred from CALIPSO lidar and IIR retrievals of semi-transparent cirrus cloud optical depths over oceans, *Atmos. Meas. Tech.*, 8, 2759–2774, <https://doi.org/10.5194/amt-8-2759-2015>, 2015.
- 980 Guzman, R., Chepfer, H., Noel, V., Vaillant de Guélis, T., Kay, J. E., Raberanto, P., Cesana, G., Vaughan, M. A., and Winker, D. M.: Direct atmosphere opacity observations from CALIPSO provide new constraints on cloud-radiation interactions: GOCCP v3.0 OPAQ Algorithm, *J. Geophys. Res. Atmos.*, 122, 1066–1085, <https://doi.org/10.1002/2016JD025946>, 2017.
- Haeffelin, M., Barthès, L., Bock, O., Boitel, C., Bony, S., Bouniol, D., Chepfer, H., Chiriaco, M., Cuesta, J., Delanoë, J.,  
985 Drobinski, P., Dufresne, J.-L., Flamant, C., Grall, M., Hodzic, A., Hourdin, F., Lapouge, F., Lemaître, Y., Mathieu, A., Morille, Y., Naud, C., Noël, V., O’Hirok, W., Pelon, J., Pietras, C., Protat, A., Romand, B., Scialom, G., and Vautard, R.: SIRTa, a ground-based atmospheric observatory for cloud and aerosol research, *Ann. Geophys.*, 23, 253–275, <https://doi.org/10.5194/angeo-23-253-2005>, 2005.
- Ham, S.-H., S. Kato, F. G. Rose, D. Winker, T. L’Ecuyer, G. G. Mace, D. Painemal, S. Sun-Mack, Y. Chen, and W. F. Miller (2017), Cloud occurrences and cloud radiative effects (CREs) from CERES-CALIPSO-CloudSat-MODIS (CCCM) and CloudSat radar-lidar (RL) products, *J. Geophys. Res. Atmos.*, 122, doi:10.1002/2017JD026725.  
990
- Hang, Y., L’Ecuyer, T. S., Henderson, D. S., Matus, A. V., and Wang, Z.: Reassessing the Effect of Cloud Type on Earth’s Energy Balance in the Age of Active Spaceborne Observations. Part II: Atmospheric Heating, 32, 6219–6236, <https://doi.org/10.1175/JCLI-D-18-0754.1>, 2019.
- 995 He, Y., Risi, C., Gao, J., Masson-Delmotte, V., Yao, T., Lai, C.-T., Ding, Y., Worden, J., Frankenberg, C., Chepfer, H., and Cesana, G.: Impact of atmospheric convection on south Tibet summer precipitation isotopologue composition using a combination of in situ measurements, satellite data, and atmospheric general circulation modeling: IMPACT OF CONVECTION ON TP ISOTOPIC, *J. Geophys. Res. Atmos.*, 120, 3852–3871, <https://doi.org/10.1002/2014JD022180>, 2015.
- 1000 Henderson, D. S., L’Ecuyer, T., Stephens, G., Partain, P., and Sekiguchi, M.: A Multisensor Perspective on the Radiative Impacts of Clouds and Aerosols, 52, 853–871, <https://doi.org/10.1175/JAMC-D-12-025.1>, 2013.

Hofer, S., Tedstone, A. J., Fettweis, X., and Bamber, J. L.: Decreasing cloud cover drives the recent mass loss on the Greenland Ice Sheet, 9, 2017.

1005 | [Hinkelman](#)

- Illingworth, A. J., Barker, H. W., Beljaars, A., Ceccaldi, M., Chepfer, H., Clerbaux, N., Cole, J., Delanoë, J., Domenech, C., Donovan, D. P., Fukuda, S., Hirakata, M., Hogan, R. J., Huenerbein, A., Kollias, P., Kubota, T., Nakajima, T., Nakajima, T. Y., Nishizawa, T., Ohno, Y., Okamoto, H., Oki, R., Sato, K., Satoh, M., Shephard, M. W., Velázquez-Blázquez, A., Wandinger, U., Wehr, T., and Zadelhoff, G.-J. van: The EarthCARE Satellite: The Next Step Forward in Global Measurements of Clouds, Aerosols, Precipitation, and Radiation, 96, 1311–1332, <https://doi.org/10.1175/BAMS-D-12-00227.1>, 2015.
- 1010 Intrieri, J. M., Fairall, C. F., Shupe, M. D., Persson, P. O. G., Andreas, E. L., Guest, P., Moritz, R. M.: An annual cycle of Arctic surface cloud forcing at SHEBA, *J. Geophys. Res.*, 107, 8039, <https://doi.org/10.1029/2000JC000439>, 2002.
- 1015 IPCC, (2021). Climate Change 2021: The Physical Science Basis. Contribution of Working Group I to the Sixth Assessment Report of the Intergovernmental Panel on Climate Change, in: Masson-Delmotte, V., Zhai, P., Pirani, A., Connors, S., L, Péan, C., Berger, S., Caud, N., Chen, Y., Goldfarb, L., Gomis, M., I, Huang, M., Leitzell, K., Lonnoy, E., Matthews, J., B, R, Maycock, T., K, Waterfield, T., Yelekçi, O., Yu, R., Zhou, B. (Eds.), Cambridge University Press. In Press.
- Kato, S., Rose, F. G., Rutan, D. A., and Charlock, T. P.: Cloud Effects on the Meridional Atmospheric Energy Budget Estimated from Clouds and the Earth's Radiant Energy System (CERES) Data, 21, 4223–4241, <https://doi.org/10.1175/2008JCLI1982.1>, 2008.
- 1020 Kato, S., Sun-Mack, S., Miller, W. F., Rose, F. G., Chen, Y., Minnis, P., and Wielicki, B. A.: Relationships among cloud occurrence frequency, overlap, and effective thickness derived from CALIPSO and CloudSat merged cloud vertical profiles, *J. Geophys. Res.*, 115, D00H28, <https://doi.org/10.1029/2009JD012277>, 2010.
- 1025 Kato, S., Loeb, N. G., Rose, F. G., Doelling, D. R., Rutan, D. A., Caldwell, T. E., Yu, L., and Weller, R. A.: Surface Irradiances Consistent with CERES-Derived Top-of-Atmosphere Shortwave and Longwave Irradiances, 26, 2719–2740, <https://doi.org/10.1175/JCLI-D-12-00436.1>, 2013.
- Kato, S., Rose, F. G., Rutan, D. A., Thorsen, T. J., Loeb, N. G., Doelling, D. R., Huang, X., Smith, W. L., Su, W., and Ham, S.-H.: Surface Irradiances of Edition 4.0 Clouds and the Earth's Radiant Energy System (CERES) Energy Balanced and Filled (EBAF) Data Product, 31, 4501–4527, <https://doi.org/10.1175/JCLI-D-17-0523.1>, 2018.
- 1030 [Kato, S., Rose, F. G., Ham, S. H., Rutan, D. A., Radkevich, A., Caldwell, T. E., et al. \(2019\). Radiative heating rates computed with clouds derived from satellite based passive and active sensors and their effects on generation of available potential energy. \*Journal of Geophysical Research: Atmospheres\*, 124, 1720–1740. <https://doi.org/10.1029/2018JD028878>](#)
- Kay, J. E., Hillman, B. R., Klein, S. A., Zhang, Y., Medeiros, B., Pincus, R., Gettelman, A., Eaton, B., Boyle, J., Marchand, R., and Ackerman, T. P.: Exposing Global Cloud Biases in the Community Atmosphere Model (CAM) Using Satellite Observations and Their Corresponding Instrument Simulators, 25, 5190–5207, <https://doi.org/10.1175/JCLI-D-11-00469.1>, 2012.
- 1035

- Kay, J. E., Deser, C., Phillips, A., Mai, A., Hannay, C., Strand, G., Arblaster, J. M., Bates, S. C., Danabasoglu, G., Edwards, J., Holland, M., Kushner, P., Lamarque, J.-F., Lawrence, D., Lindsay, K., Middleton, A., Munoz, E., Neale, R., Oleson, K., Polvani, L., and Vertenstein, M.: The Community Earth System Model (CESM) Large Ensemble Project: A Community Resource for Studying Climate Change in the Presence of Internal Climate Variability, 96, 1333–1349, <https://doi.org/10.1175/BAMS-D-13-00255.1>, 2015.
- King, J. C., Gadian, A., Kirchgassner, A., Kuipers Munneke, P., Lachlan-Cope, T. A., Orr, A., Reijmer, C., van den Broeke, M. R., van Wessem, J. M., and Weeks, M.: Validation of the summertime surface energy budget of Larsen C Ice Shelf (Antarctica) as represented in three high-resolution atmospheric models: Surface energy budget of Larsen C, J. Geophys. Res. Atmos., 120, 1335–1347, <https://doi.org/10.1002/2014JD022604>, 2015.
- Kopp, R. E., Kemp, A. C., Bittermann, K., Horton, B. P., Donnelly, J. P., Gehrels, W. R., Hay, C. C., Mitrovica, J. X., Morrow, E. D., and Rahmstorf, S.: Temperature-driven global sea-level variability in the Common Era, Proc Natl Acad Sci USA, 113, E1434–E1441, <https://doi.org/10.1073/pnas.1517056113>, 2016.
- Kwok, R. and Untersteiner, N.: The thinning of Arctic sea ice, Physics Today, 64, 36–41, <https://doi.org/10.1063/1.3580491>, 2011.
- Lacour, A., Chepfer, H., Miller, N. B., Shupe, M. D., Noel, V., Fettweis, X., Gallee, H., Kay, J. E., Guzman, R., and Cole, J.: How Well Are Clouds Simulated over Greenland in Climate Models? Consequences for the Surface Cloud Radiative Effect over the Ice Sheet, J. Climate, 31, 9293–9312, <https://doi.org/10.1175/JCLI-D-18-0023.1>, 2018.
- L’Ecuyer, T. S., Wood, N. B., Haladay, T., Stephens, G. L., and Stackhouse, P. W.: Impact of clouds on atmospheric heating based on the R04 CloudSat fluxes and heating rates data set, J. Geophys. Res., 113, D00A15, <https://doi.org/10.1029/2008JD009951>, 2008.
- L’Ecuyer, T. S., Hang, Y., Matus, A. V., and Wang, Z.: Reassessing the Effect of Cloud Type on Earth’s Energy Balance in the Age of Active Spaceborne Observations. Part I: Top of Atmosphere and Surface, 32, 6197–6217, <https://doi.org/10.1175/JCLI-D-18-0753.1>, 2019.
- Lindzen, R. S. and Choi, Y.-S.: The Iris Effect: A Review, Asia-Pacific J Atmos Sci, <https://doi.org/10.1007/s13143-021-00238-1>, 2021.
- Liu, Y., Ackerman, S. A., Maddux, B. C., Key, J. R., and Frey, R. A.: Errors in Cloud Detection over the Arctic Using a Satellite Imager and Implications for Observing Feedback Mechanisms, 23, 1894–1907, <https://doi.org/10.1175/2009JCLI3386.1>, 2010.
- Loeb, N. G., S. Kato, K. Loukachine, and N. Manalo-Smith (2005), *Angular distribution models for top-of-atmosphere radiative flux estimation from the Clouds and the Earth’s Radiant Energy System instrument on the Terra satellite. Part I: Methodology*, J. Atmos. Ocean. Technol., 22(4), 338–351, doi:10.1175/JTECH1712.1.
- Loeb, N. G., S. Kato, K. Loukachine, N. Manalo-Smith, and D. R. Doelling (2007), *Angular distribution models for top-of-atmosphere radiative flux estimation from the Clouds and the Earth’s Radiant Energy System instrument on the Terra satellite. Part II: Validation*, J. Atmos. Ocean. Technol., 24(4), 564–584, doi:10.1175/jtech1983.1.
- Loeb, N. G., Wang, H., Cheng, A., Kato, S., Fasullo, J. T., Xu, K.-M., and Allan, R. P.: Observational constraints on atmospheric and oceanic cross-equatorial heat transports: revisiting the precipitation asymmetry problem in climate models, Clim Dyn, 46, 3239–3257, <https://doi.org/10.1007/s00382-015-2766-z>, 2016.

- 1075 [Minnis, P., and Coauthors, 2010: CERES Edition 3 cloud retrievals. 13<sup>th</sup> Conf. on Atmospheric Radiation, Portland, OR, Amer. Meteor. Soc., 5.4, <https://ams.confex.com/ams/pdfpapers/171366.pdf>.](#)  
[Mülmenstädt, J., Sourdeval, O., Henderson, D. S., L'Ecuyer, T. S., Unglaub, C., Jungandreas, L., Böhm, C., Russell, L. M., and Quaas, J.: Using CALIOP to estimate cloud-field base height and its uncertainty: the Cloud Base Altitude Spatial Extrapolator \(CBASE\) algorithm and dataset \(1\), <https://doi.org/10.1594/WDCC/CBASE>, 2018.](#)
- 1080 Norris, J. R., Allen, R. J., Evan, A. T., Zelinka, M. D., O'Dell, C. W., and Klein, S. A.: Evidence for climate change in the satellite cloud record, *Nature*, 536, 72–75, <https://doi.org/10.1038/nature18273>, 2016.  
Ohmura, A., Dutton, E. G., Forgan, B., Fröhlich, C., Gilgen, H., Hegner, H., Heimo, A., König-Langlo, G., McArthur, B., and Müller, G.: Baseline Surface Radiation Network (BSRN/WCRP): New precision radiometry for climate research, 79, 2115–2136, 1998.
- 1085 Prata, A. J.: A new long-wave formula for estimating downward clear-sky radiation at the surface, *Q.J Royal Met. Soc.*, 122, 1127–1151, <https://doi.org/10.1002/qj.49712253306>, 1996.  
Ramanathan, V.: Interactions between ice-albedo, lapse-rate and cloud-top feedbacks: An analysis of the nonlinear response of a GCM climate model, 34, 1885–1897, 1977.  
Ramanathan, V., Cess, R. D., Harrison, E. F., Minnis, P., and Barkstrom, B. R.: Cloud-Radiative Forcing and Climate: Results from the Earth Radiation Budget Experiment, 243, 8, 1989.
- 1090 Roesch, A., Wild, M., Ohmura, A., Dutton, E. G., Long, C. N., and Zhang, T.: Assessment of BSRN radiation records for the computation of monthly means, *Atmos. Meas. Tech.*, 4, 339–354, <https://doi.org/10.5194/amt-4-339-2011>, 2011.  
[Rienecker, M. M., Todling, R., Bacmeister, J., Takacs, L., Liu, H. C., Gu, W., et al. \(2008\). The GEOS 5 data assimilation system: Documentation of versions 5.0.1, 5.1.0, and 5.2.0. NASA Technical Report Series on Global Modeling and Data Assimilation, Vol. 27, NASA/TM 2008 105606, 97 pp.](#)
- 1095 [Rojas Muñoz, O. J., Chiriaco, M., Bastin, S., & Ringard, J. \(2021\). Estimation of the terms acting on local 1 h surface temperature variations in Paris region: the specific contribution of clouds. \*Atmospheric Chemistry and Physics\*, 21\(20\), 15699-15723.](#)  
Rousset, C., Vancoppenolle, M., Madec, G., Fichefet, T., Flavoni, S., Barthélemy, A., Benshila, R., Chanut, J., Levy, C., Masson, S., and Vivier, F.: The Louvain-La-Neuve sea ice model LIM3.6: global and regional capabilities, *Geosci. Model Dev.*, 8, 2991–3005, <https://doi.org/10.5194/gmd-8-2991-2015>, 2015.  
[Rutan, D. A., Kato, S., Doelling, D. R., Rose, F. G., Nguyen, L. T., Caldwell, T. E., and Loeb, N. G.: CERES Synoptic Product: Methodology and Validation of Surface Radiant Flux, 32, 1121–1143, <https://doi.org/10.1175/JTECH-D-14-00165.1>, 2015.](#)
- 1105 [Sassen, K., and Z. Wang \(2008\). Classifying clouds around the globe with the CloudSat radar: 1-year of results, \*Geophys. Res. Lett.\*, 35, L04805, doi:10.1029/2007GL032591.](#)  
Scott, R. C., Lubin, D., Vogelmann, A. M., and Kato, S.: West Antarctic Ice Sheet Cloud Cover and Surface Radiation Budget from NASA A-Train Satellites, *J. Climate*, 30, 6151–6170, <https://doi.org/10.1175/JCLI-D-16-0644.1>, 2017.  
Shupe, M. D. and Intrieri, J. M.: Cloud Radiative Forcing of the Arctic Surface: The Influence of Cloud Properties, Surface Albedo, and Solar Zenith Angle, 17, 13, [https://doi.org/10.1175/1520-0442\(2004\)017<0616:CRFOTA>2.0.CO;2](https://doi.org/10.1175/1520-0442(2004)017<0616:CRFOTA>2.0.CO;2), 2004.
- 1110

- Shupe, M. D., Turner, D. D., Walden, V. P., Bennartz, R., Cadeddu, M. P., Castellani, B. B., Cox, C. J., Hudak, D. R., Kulie, M. S., Miller, N. B., Neely, R. R., Neff, W. D., and Rowe, P. M.: High and Dry: New Observations of Tropospheric and Cloud Properties above the Greenland Ice Sheet, 94, 169–186, <https://doi.org/10.1175/BAMS-D-11-00249.1>, 2013.
- 1115 Stephens, G. L., Vane, D. G., Tanelli, S., Im, E., Durden, S., Rokey, M., Reinke, D., Partain, P., Mace, G. G., Austin, R., L’Ecuyer, T., Haynes, J., Lebsock, M., Suzuki, K., Waliser, D., Wu, D., Kay, J., Gettelman, A., Wang, Z., and Marchand, R.: CloudSat mission: Performance and early science after the first year of operation, 113, <https://doi.org/10.1029/2008JD009982>, 2008.
- 1120 [Stephens, G. L., Vane, D. G., Boain, R. J., Mace, G. G., Sassen, K., Wang, Z., Illingworth, A. J., O’connor, E. J., Rossow, W. B., Durden, S. L., Miller, S. D., Austin, R. T., Benedetti, A., Mitrescu, C., and the CloudSat Science Team: THE CLOUDSAT MISSION AND THE A-TRAIN: A New Dimension of Space-Based Observations of Clouds and Precipitation, Bull. Amer. Meteor. Soc., 83, 1771–1790, <https://doi.org/10.1175/BAMS-83-12-1771>, 2002.](#)
- Stroeve, J. C., Serreze, M. C., Holland, M. M., Kay, J. E., Maslanik, J., and Barrett, A. P.: The Arctic’s rapidly shrinking sea ice cover: a research synthesis, Climatic Change, 110, 1005–1027, <https://doi.org/10.1007/s10584-011-0101-1>, 2012.
- 1125 Stubenrauch, C. J., Rossow, W. B., Kinne, S., Ackerman, S., Cesana, G., Chepfer, H., Girolamo, L. D., Getzewich, B., Guignard, A., Heidinger, A., Maddux, B. C., Menzel, W. P., Minnis, P., Pearl, C., Platnick, S., Poulsen, C., Riedi, J., Sun-Mack, S., Walther, A., Winker, D., Zeng, S., and Zhao, G.: ASSESSMENT OF GLOBAL CLOUD DATASETS FROM SATELLITES, 20, 2013.
- Stubenrauch W. B. Rossow, and S. Kinne, 2012: Assessment of global cloud datasets from satellites: A project of the World Climate Research Programme Global Energy and Water Cycle Experiment (GEWEX) Radiation Panel. WCRP Rep. 1130 23/2012, 176 pp. [Available online at [www.wcrp-climate.org/documents/GEWEX\\_Cloud\\_Assessment\\_2012.pdf](http://www.wcrp-climate.org/documents/GEWEX_Cloud_Assessment_2012.pdf).]
- Taylor, K. E., Crucifix, M., Braconnot, P., Hewitt, C. D., Doutriaux, C., Broccoli, A. J., Mitchell, J. F. B., and Webb, M. J.: Estimating Shortwave Radiative Forcing and Response in Climate Models, 20, 2530–2543, <https://doi.org/10.1175/JCLI4143.1>, 2007.
- 1135 Vaillant de Guélis, T., Chepfer, H., Noel, V., Guzman, R., Dubuisson, P., Winker, D. M., and Kato, S.: The link between outgoing longwave radiation and the altitude at which a spaceborne lidar beam is fully attenuated, Atmos. Meas. Tech., 10, 4659–4685, <https://doi.org/10.5194/amt-10-4659-2017>, 2017a.
- Vaillant de Guélis, T., Chepfer, H., Noel, V., Guzman, R., Winker, D. M., and Plougonven, R.: Using Space Lidar Observations to Decompose Longwave Cloud Radiative Effect Variations Over the Last Decade: Space lidar decomposes LWCRE variations, Geophys. Res. Lett., 44, 11,994–12,003, <https://doi.org/10.1002/2017GL074628>, 2017b.
- 1140 Vaillant de Guélis, T., Chepfer, H., Guzman, R., Bonazzola, M., Winker, D. M., and Noel, V.: Space lidar observations constrain longwave cloud feedback, Sci Rep, 8, 16570, <https://doi.org/10.1038/s41598-018-34943-1>, 2018.
- Van Tricht, K., Lhermitte, S., Lenaerts, J. T. M., Gorodetskaya, I. V., L’Ecuyer, T. S., Noël, B., van den Broeke, M. R., Turner, D. D., and van Lipzig, N. P. M.: Clouds enhance Greenland ice sheet meltwater runoff, Nat Commun, 7, 10266, <https://doi.org/10.1038/ncomms10266>, 2016.
- 1145 [Vaughan, M., Pitts, M., Trepte, C., Winker, D., Detweiler, P., Garnier, A., Getzewich, B., Hunt, W., Lambeth, J., Lee, K.-P., Lucker, P., Murray, T., Rodier, S., Tremas, T., Bazureau, A. and Pelon, J. \(2018\): Cloud-Aerosol LIDAR Infrared Pathfinder Satellite Observations \(CALIPSO\) data management system data products catalog, Release 4.30, NASA Langley Research](#)

- 1150 Winker, D. M., Pelon, J., Jr, J. A. C., Ackerman, S. A., Charlson, R. J., Colarco, P. R., Flamant, P., Fu, Q., Hoff, R. M., Kittaka, C., Kubar, T. L., Treut, H. L., McCormick, M. P., Mégie, G., Poole, L., Powell, K., Treppe, C., Vaughan, M. A., and Wielicki, B. A.: A Global 3D View of Aerosols and Clouds, 20, 2010.  
Zelinka, M. D., Klein, S. A., and Hartmann, D. L.: Computing and Partitioning Cloud Feedbacks Using Cloud Property Histograms. Part I: Cloud Radiative Kernels, J. Climate, 25, 3715–3735, <https://doi.org/10.1175/JCLI-D-11-00248.1>, 2012a.
- 1155 Zelinka, M. D., Klein, S. A., and Hartmann, D. L.: Computing and Partitioning Cloud Feedbacks Using Cloud Property Histograms. Part II: Attribution to Changes in Cloud Amount, Altitude, and Optical Depth, J. Climate, 25, 3736–3754, <https://doi.org/10.1175/JCLI-D-11-00249.1>, 2012b.

1160



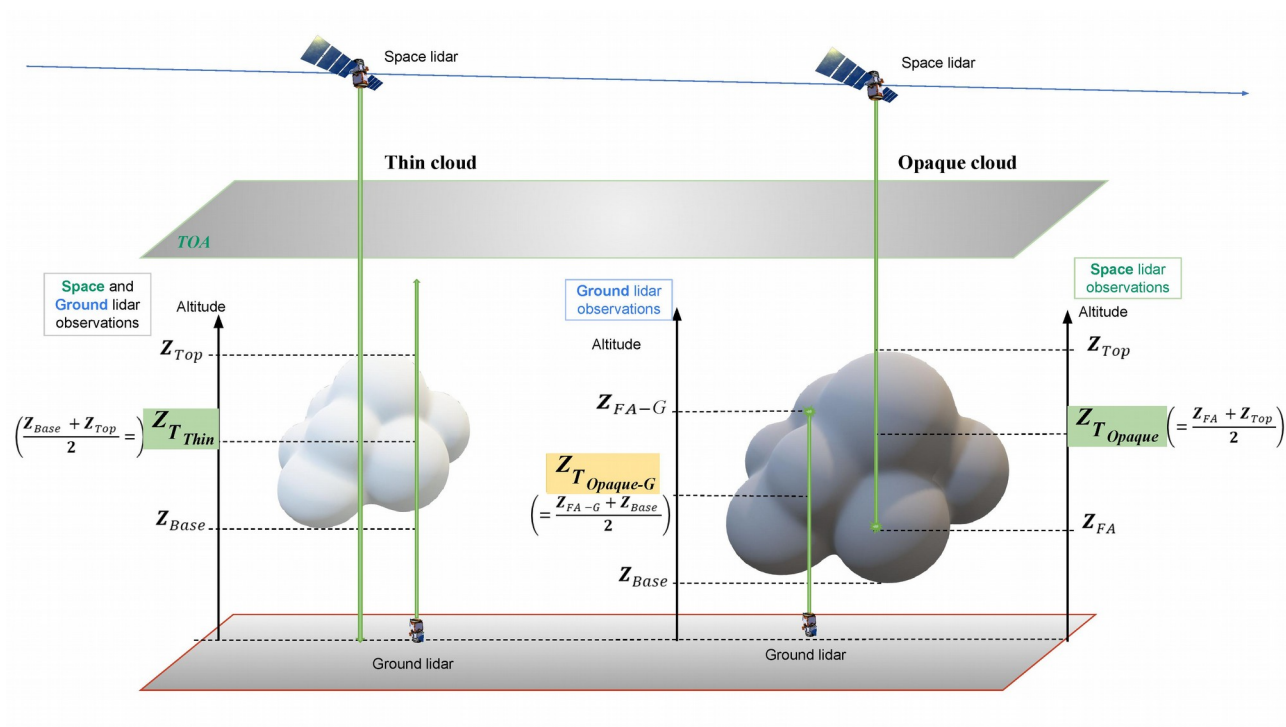


Figure 1: Schematic of cloud altitudes seen from space lidar and from a ground based lidar in an atmospheric column containing thin cloud only (left) and opaque cloud only (right). The altitudes used to retrieve the surface LW CRE from CALIPSO-GOCCP are reported in green.

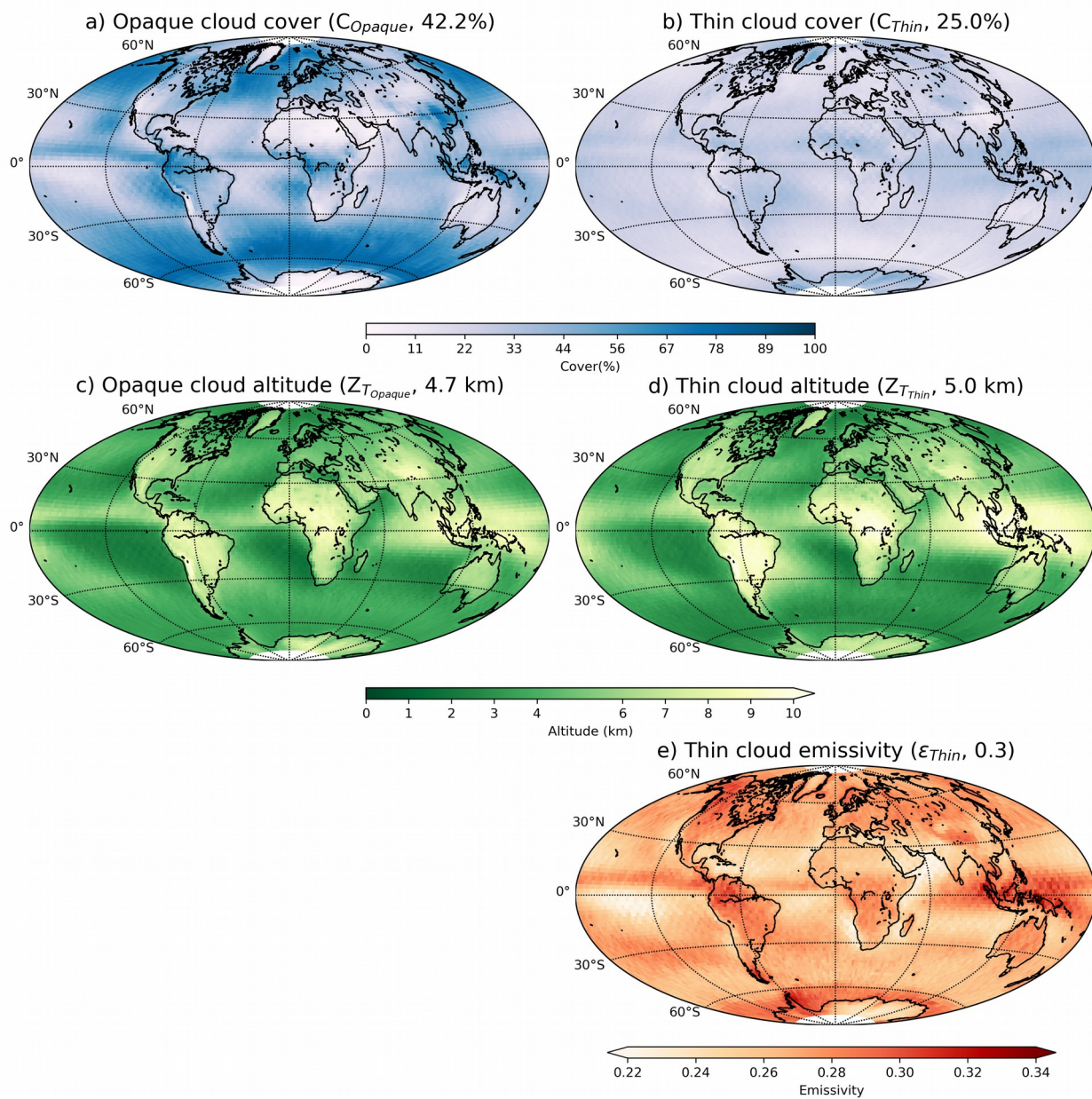


Figure 2: Maps of a) opaque cloud cover  $C_{Opaque}$ , b) thin cloud cover  $C_{Thin}$ , c) opaque cloud altitude  $Z_{T_{Opaque}}$ , d) thin cloud altitude  $Z_{T_{Thin}}$  and e) thin cloud emissivity  $\epsilon_{Thin}$ . Global mean are reported in parentheses. Build from CALIPSO-GOCCP v3.1.2 over 2008–2020.

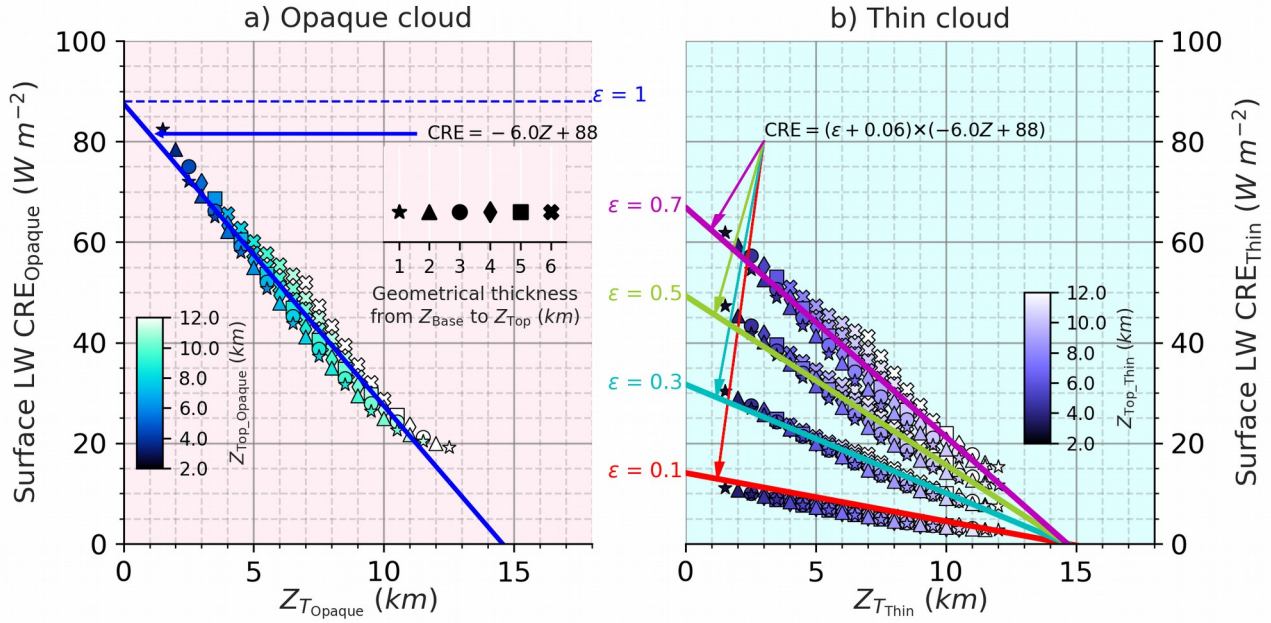


Figure 3: Linear relationships derived from 1D radiative transfer computations between the surface LW CRE and the cloud altitude for a single overcast column containing: a) an opaque cloud above a thin cloud, both moving in altitude, and b) a thin cloud of emissivity 0.1 (red), 0.3 (cyan), 0.5 (green) and 0.7 (pink). These linear relationships (solid lines) are derived from direct radiative transfer computations (dots). Each dot represents the result of one radiative transfer computation. The color of dots represents the cloud top altitude (2 km [dark] – 13 km [bright]) and the size of dots the geometrical thickness from the cloud base to cloud top (1 km [small] – 6 km and above [large]). The atmospheric state is taken from ERA Interim reanalysis for January at a latitude of 39° N over ocean.

# Radiative transfer simulations over ocean : Tropics

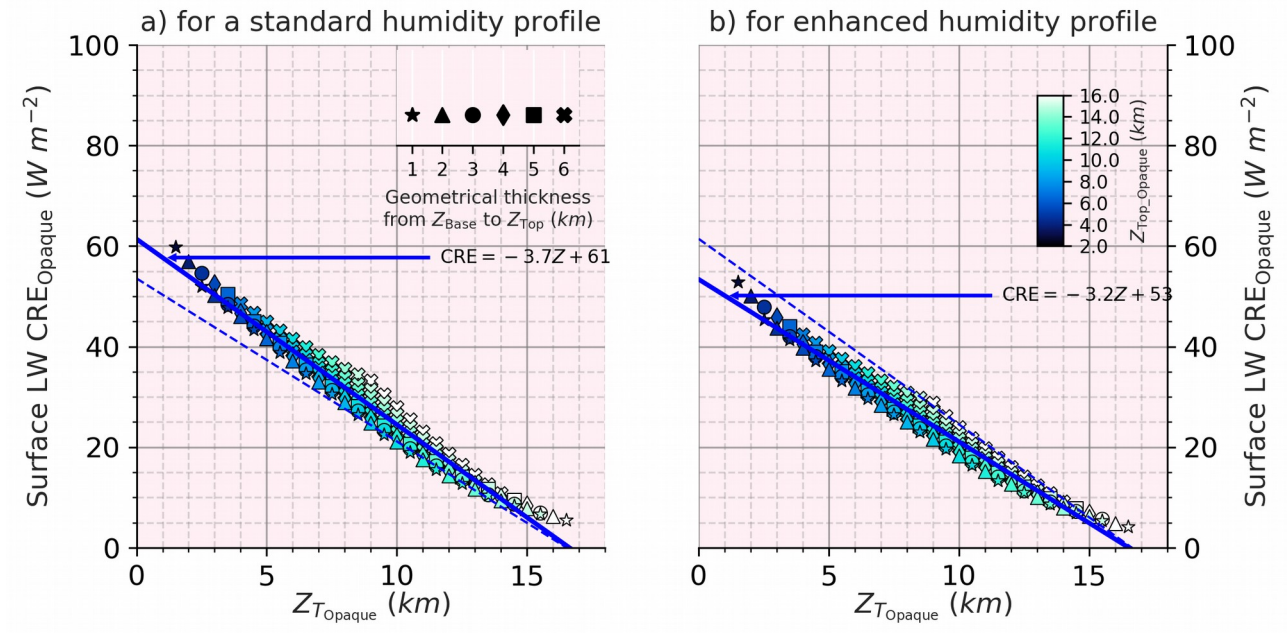
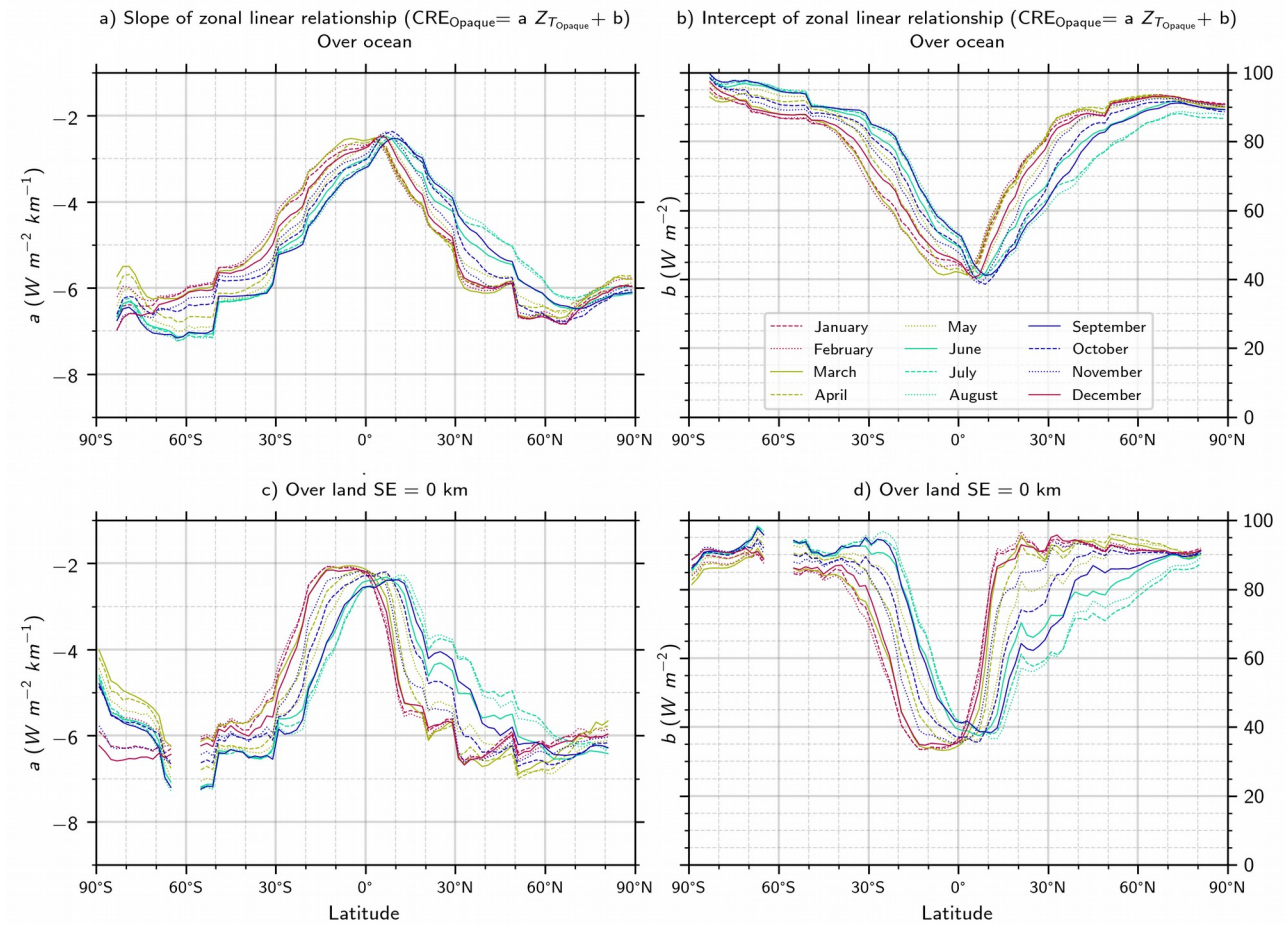


Figure 4: Same as Fig. 3a for: a) a standard humidity profile and b) enhanced humidity profile. Both in the tropics [30° S–30° N].





**Figure 5: Coefficients of the linear relationships derived from 1D radiative transfer computations between the surface LW CRE and the cloud altitude for all latitudes and seasons : a) the slope of the relationships over ocean, b) intercept of the relationships over ocean, c) the slope of the relationships over land and, d) intercept of the relationships over land.**

Radiative transfer simulations for different surface elevations  
Opaque cloud over land : January, Latitude 39° N

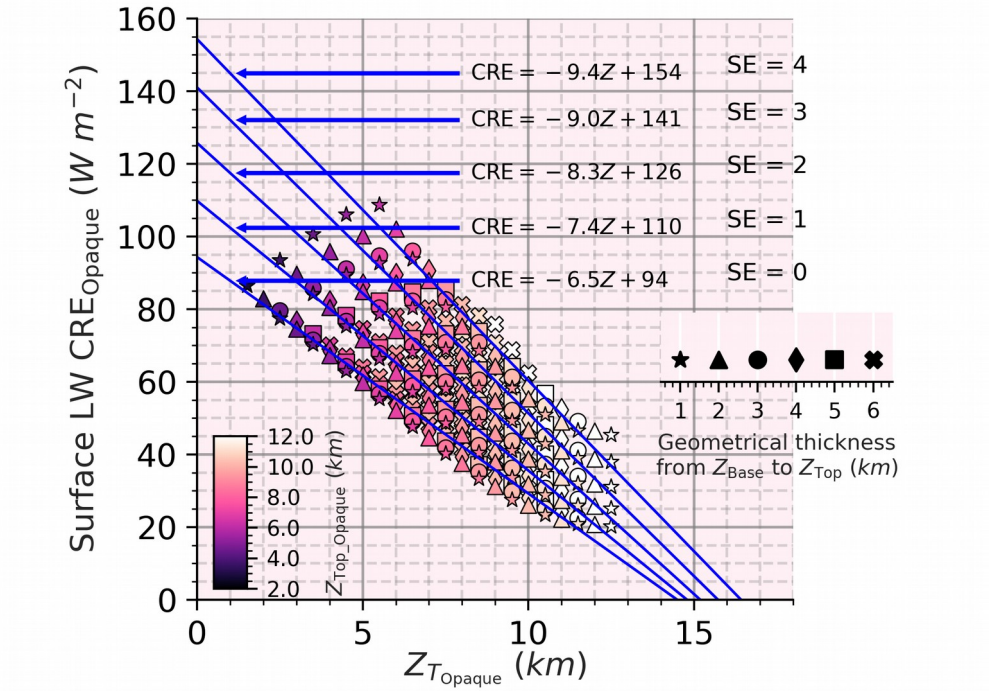
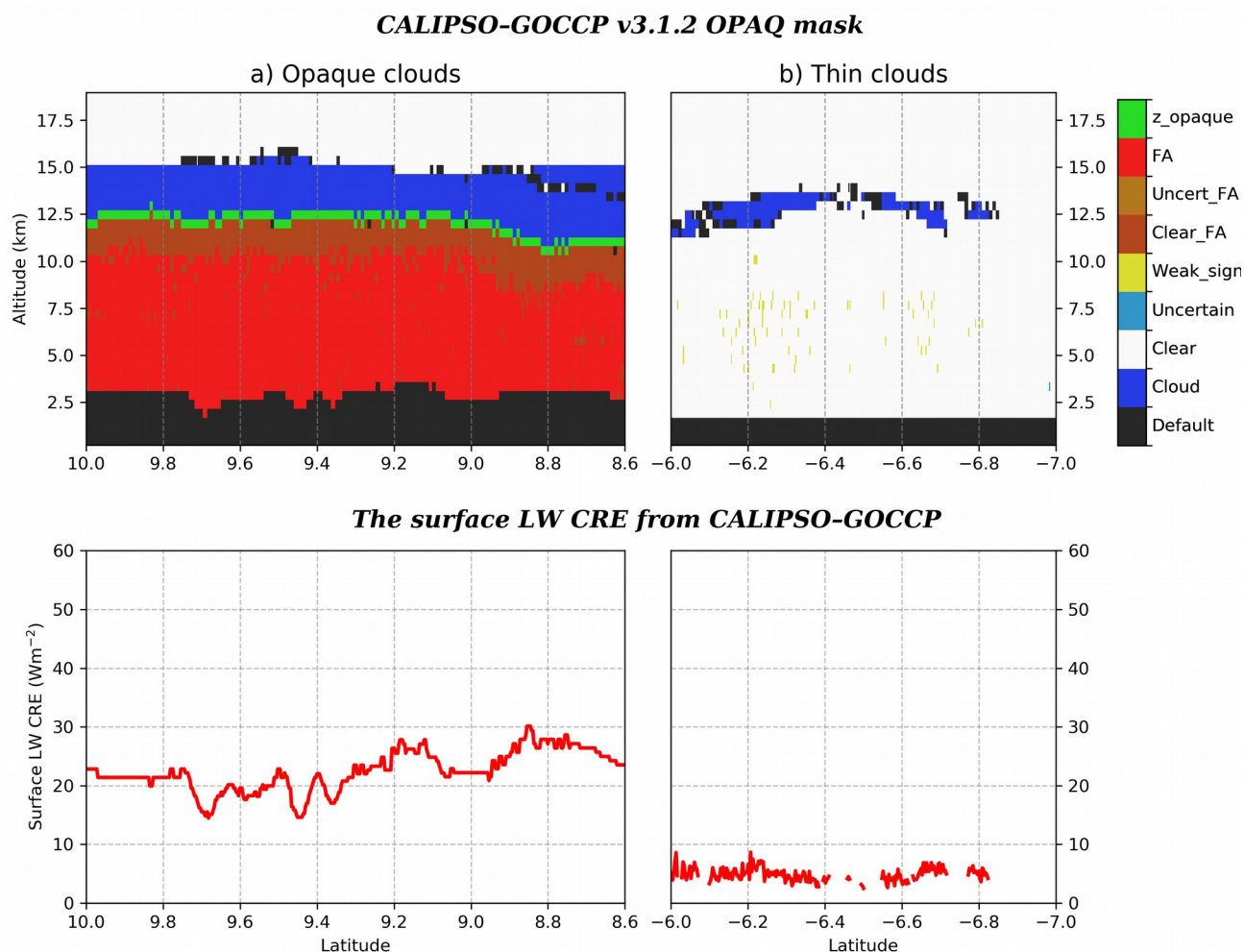
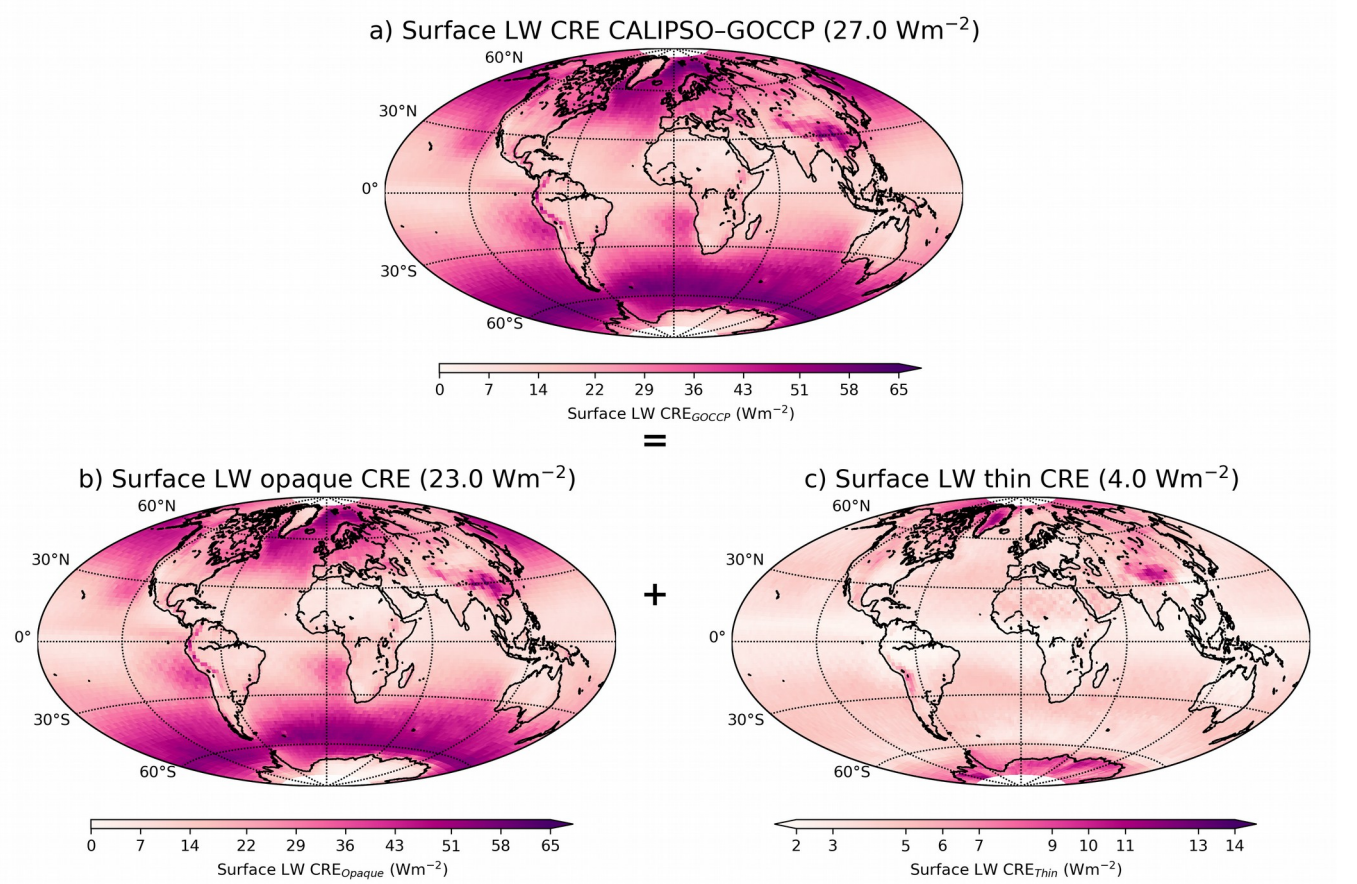


Figure 6: Sensitivity of the surface LW opaque CRE to the surface elevation (SE) : Same as Fig. 3a but over land and for different values of SE : SE = 0 (sea level), SE = 1 km, SE = 2 km, SE = 3 km, SE = 4 km for January at a latitude of 39° N.



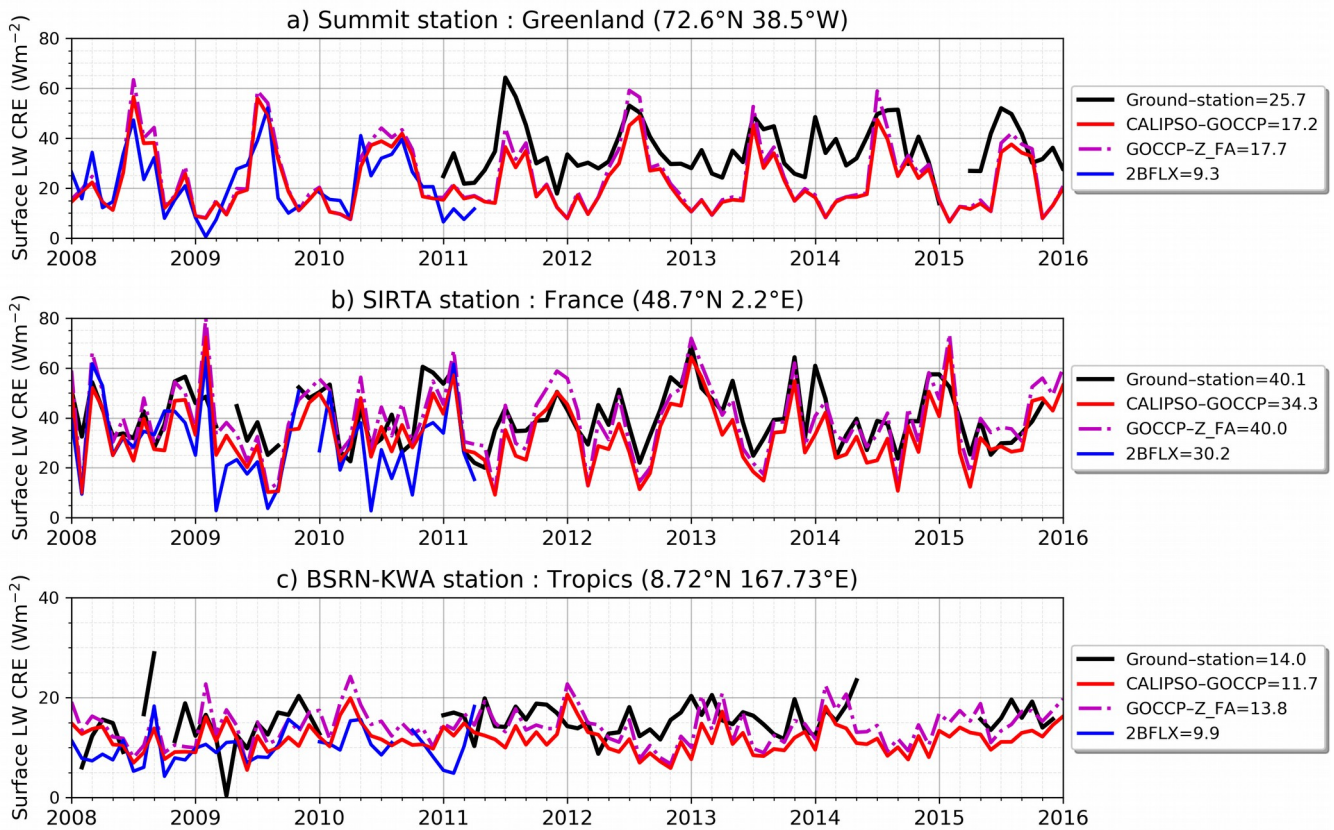
**Figure 7:** Pieces of CALIPSO orbit passing over Africa the 11<sup>th</sup> August 2010 at 23 h 02 min 38 sec. Opaque clouds (left column) and, thin clouds (right column). Top line) Vertical feature mask from the product CALIPSO-GOCCP-OPAQ (Guzman et al., 20017), the black areas below 4km correspond to land. Bottom line) Surface LW CRE from CALIPSO-GOCCP.

1230



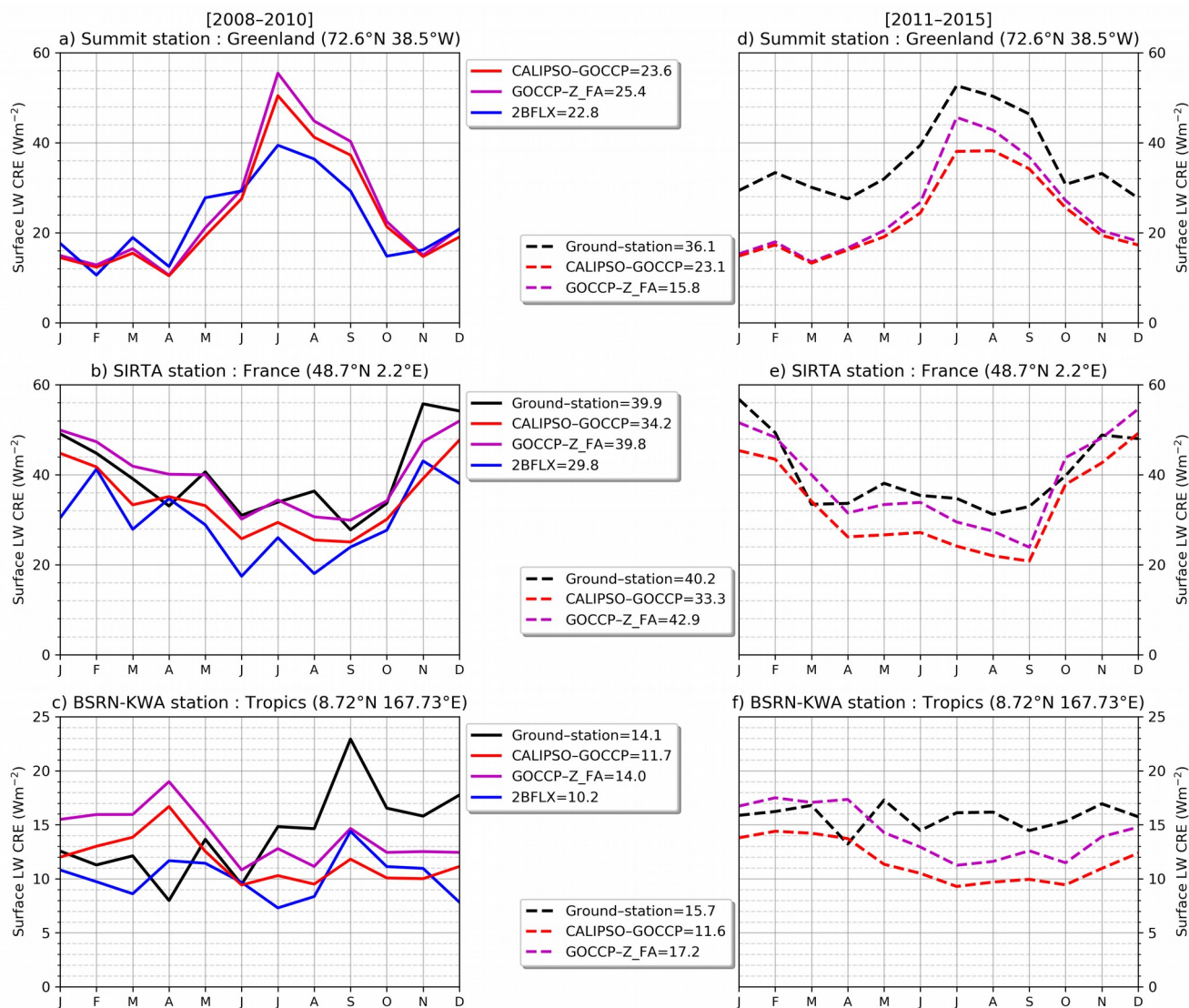
**Figure 8: Maps of the surface LW CRE: a) all clouds, b) opaque clouds, and c) thin clouds. These surface LW CRE are built from CALIPSO–GOCCP v3.1.2 dataset (Fig. 2) and radiative transfer computations (Figs. 4–7, A1). The surface LW CRE is averaged over 2008–2020. Note that the color scale is different in c).**





1235 **Figure 9: Comparisons between the surface LW CRE derived from ground-stations measurements and from satellites in three**  
**locations : a) polar region at Greenland Summit site, b) mid-latitudes at Sirta site, and c) tropics at KWA site. Mean values**  
**reported in the legend are computed only over the time period when all products are available e.g. only for months (JFMA 2011)**  
**for Greenland Summit mean values. The locations of the three sites are reported in Fig. 14. Note that the y-axis scale is different in**  
**each subplot.**

1240



1245 **Figure 10:** Same as Fig. 9 but in mean seasonal cycles. Left column corresponds to 2008–2010 and right column corresponds to 2011–2015. Note that the y-axis scale is different in each subplot.

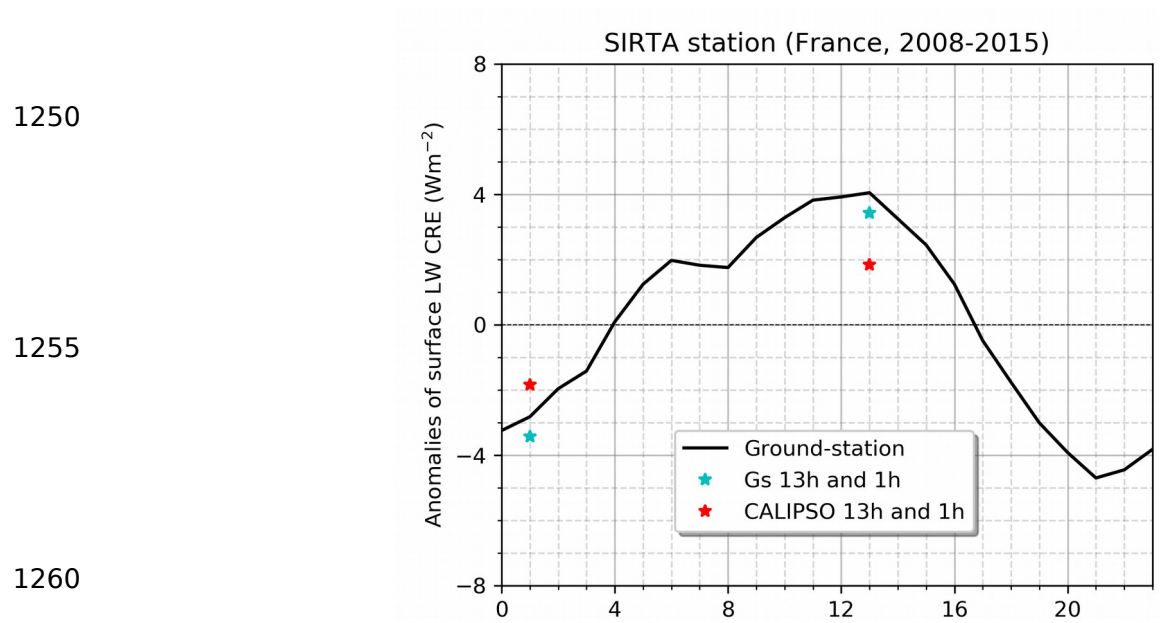


**Figure 11:** Same as Fig. 9b but in the anomaly of diurnal cycles over 2008–2015.

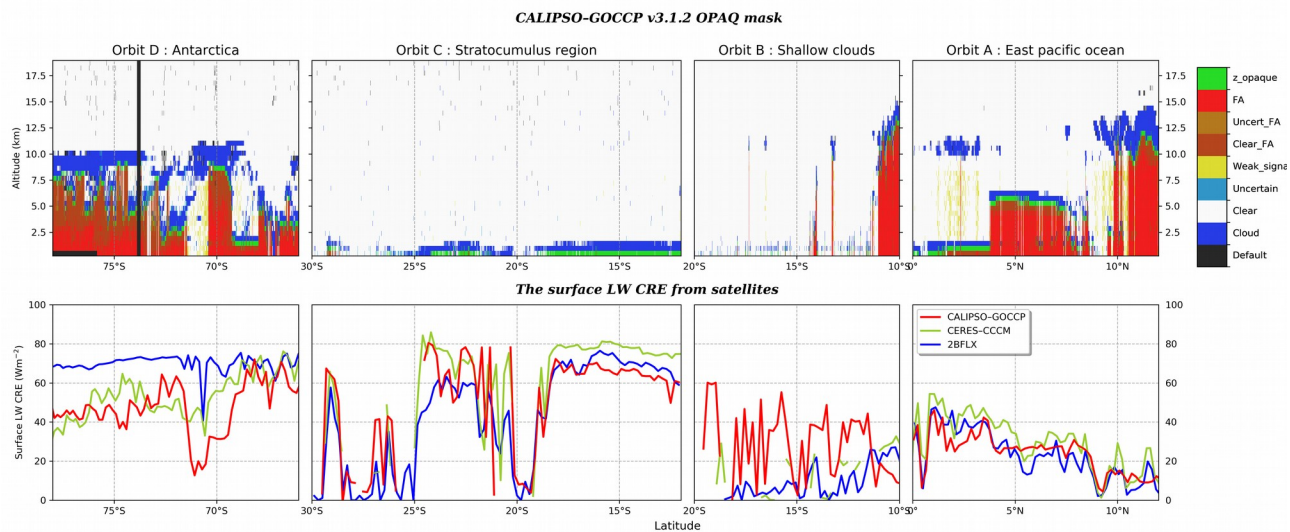


Figure 12: Pieces of CALIPSO orbits passing over: A) east Pacific ocean the 17<sup>th</sup> October at 8 h 21 min 48 sec, B) shallow clouds region in the Pacific ocean the 5<sup>th</sup> April at 12 h 55 min 34 sec, C) stratocumulus region the 13<sup>th</sup> July at 6 h 48 min 37 sec and D) Antarctica the 21<sup>st</sup> September at 3 h 9 min 46 sec all for the year 2008. Top line) Vertical feature mask from the product CALIPSO–GOCCP–OPAQ (Guzman et al., 20017), the black areas below 4km correspond to land. Bottom line) Surface LW CRE of the three satellite products. The location of the pieces of orbit (A, B, C, D) are reported in Figure 14

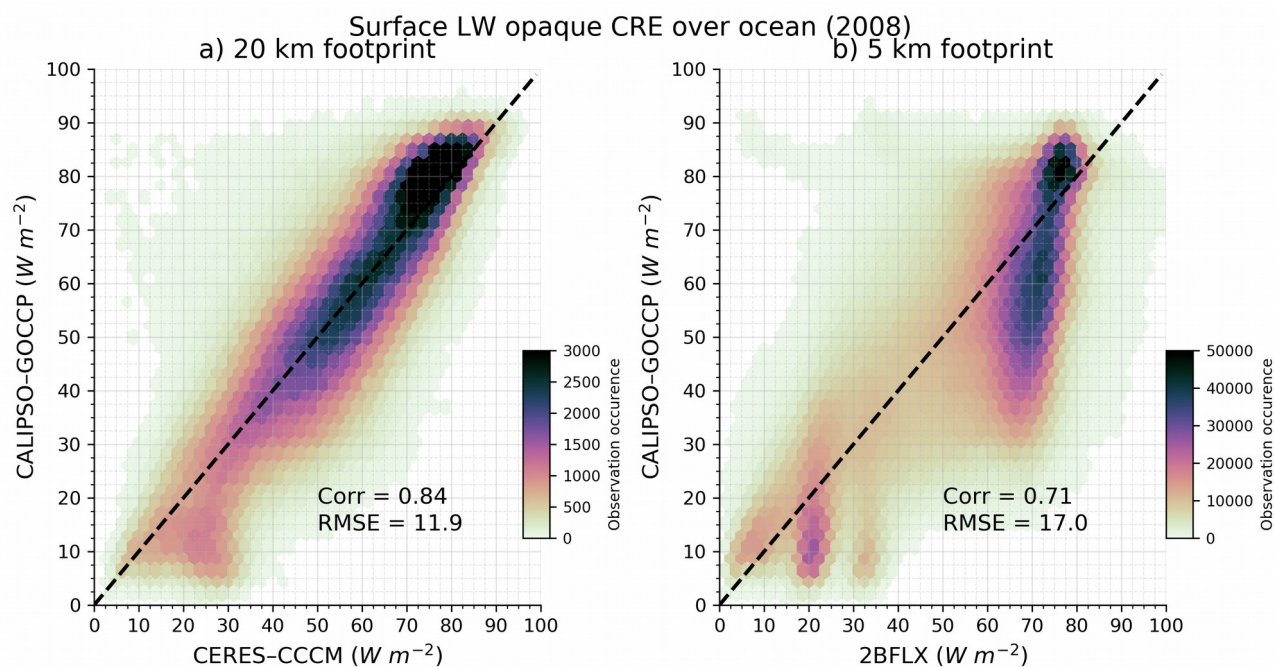


Figure 13: Instantaneous collocated surface LW opaque CRE at footprint scale: a) CALIPSO–GOCCP as a function of CERES–CCCM , b) CALIPSO–GOCCP as a function of 2BFLX. We only consider CERES (CloudSat) footprints where all CALIPSO footprints falling within the CERES (CloudSat) footprints are opaque and which contain at least 40 (10) profiles. Based on collocated observations over ocean in 2008.



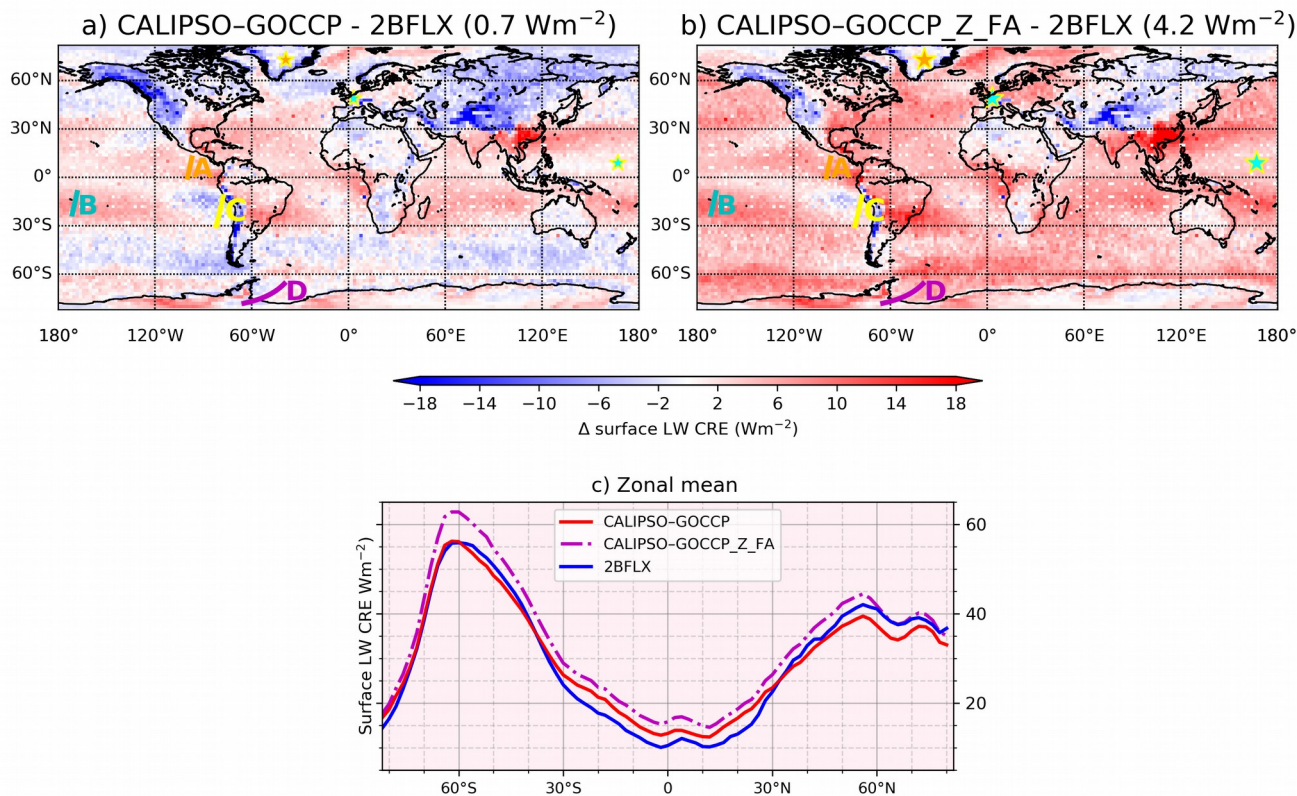
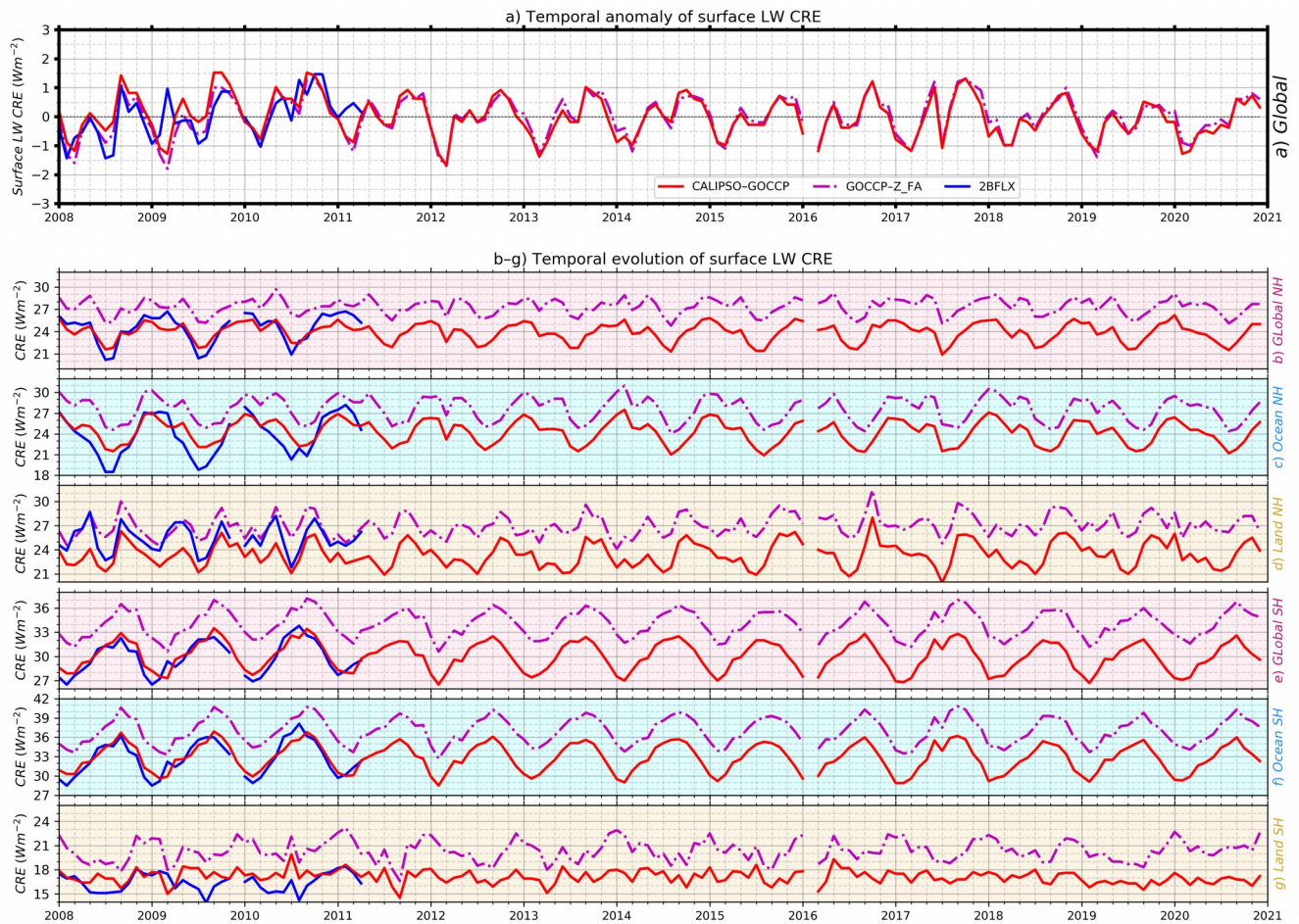
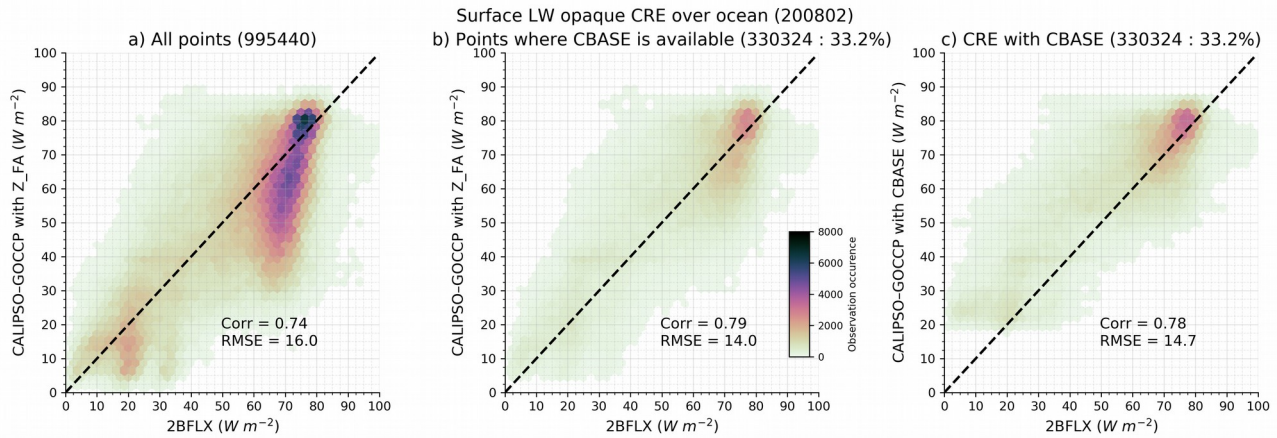


Figure 14: Maps of differences in the surface LW CRE a) CALIPSO-GOCCP minus 2BFLX, b) GOCCP\_Z\_FA minus 2BFLX, and c) zonal means of the two satellite products. Data are averaged over 2008–2010. Locations of the three ground-based sites and pieces of orbits are reported in the maps.

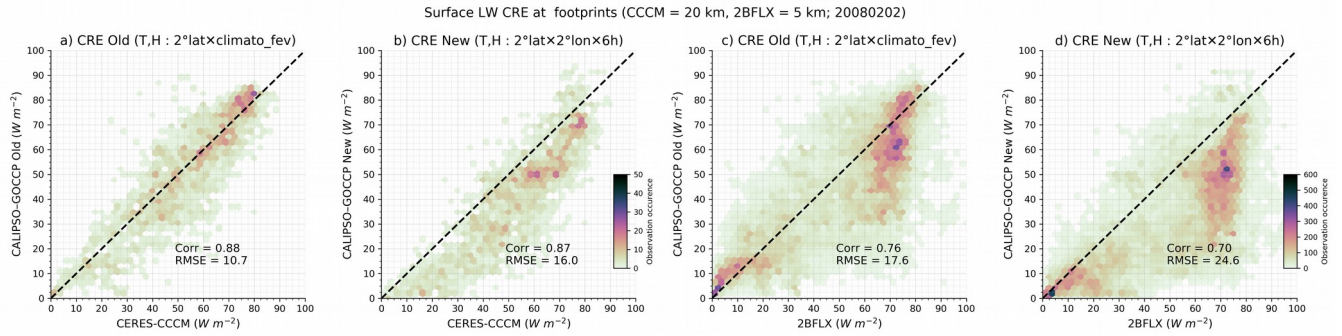


**Figure 15: a) Time series of global surface LW CRE anomalies. b-f) Time series of surface LW CREs over all NH, ocean NH, land NH, all SH, ocean SH, land SH. In a) the anomaly is defined as the global average for each month of each product minus its own average over the whole time serie. Note that the y-axis scale is different in each subplot.**



**Figure 16: Surface LW CRE derived from CALIPSO-GOCCP as a function of the one derived from 2BFLX. a) CALIPSO-GOCCP surface LW CRE (y axis) computed using the altitude of full lidar attenuation b) same as (a) but containing only the sub-sample of CALIPSO profiles where cloud base-height values are available from Mülmenstädt et al. (2018) c) same as b) but the CALIPSO-GOCCP surface LW CRE is computed using the cloud base-height values from Mülmenstädt et al. (2018) instead of the altitude of lidar full attenuation. The color scale indicates the number of occurrences at 5km resolution (footprint scale of CloudSat) over ocean in February 2008.**





1310 **Figure 17: Distribution of the Surface LW CRE: a) CALIPSO-GOCCP retrieved using monthly mean temperature/humidity profiles as a function of CERES-CCCM with data at 20 km resolution (CERES SSF footprint), b) same as (a) but CALIPSO-GOCCP retrieved using sub-daily temperature/humidity profiles, c,d) same as (a,b) but for 2BFLX instead of CERES-CCCM and using data at 5 km resolution (CloudSat resolution).**

Radiative transfer simulations over land : January, Latitude 39° N

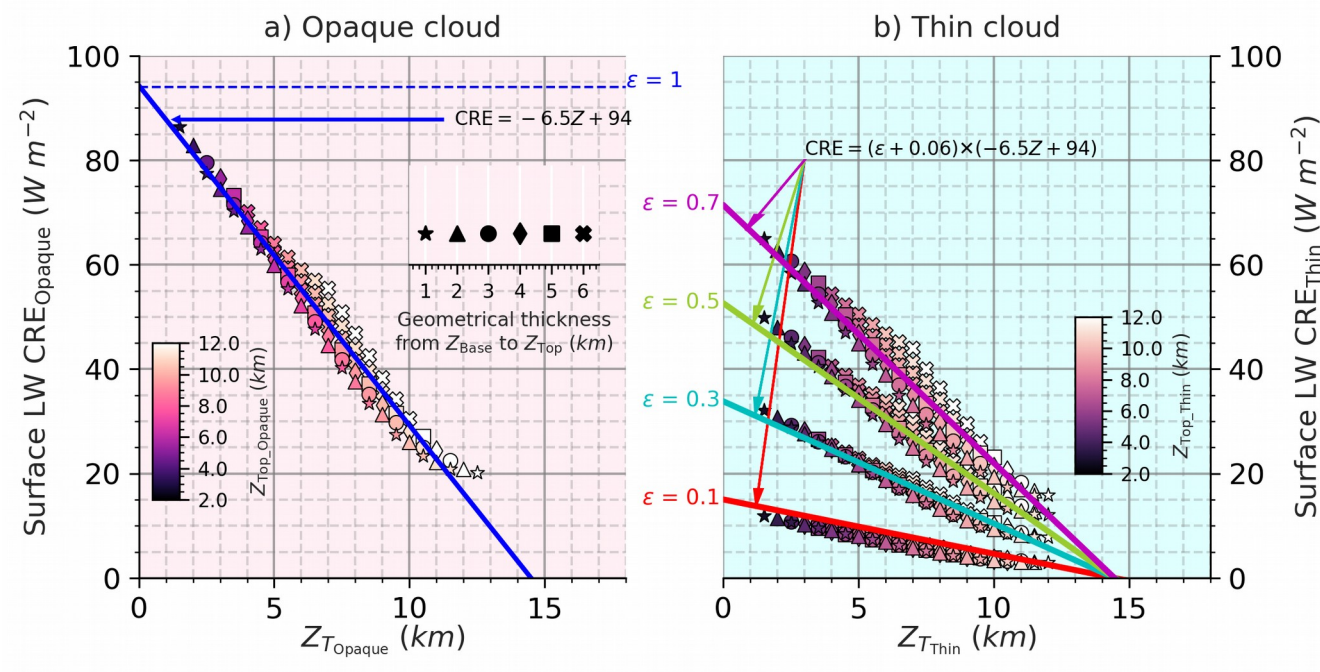


Figure A1: Same as Fig. 3 but over land.

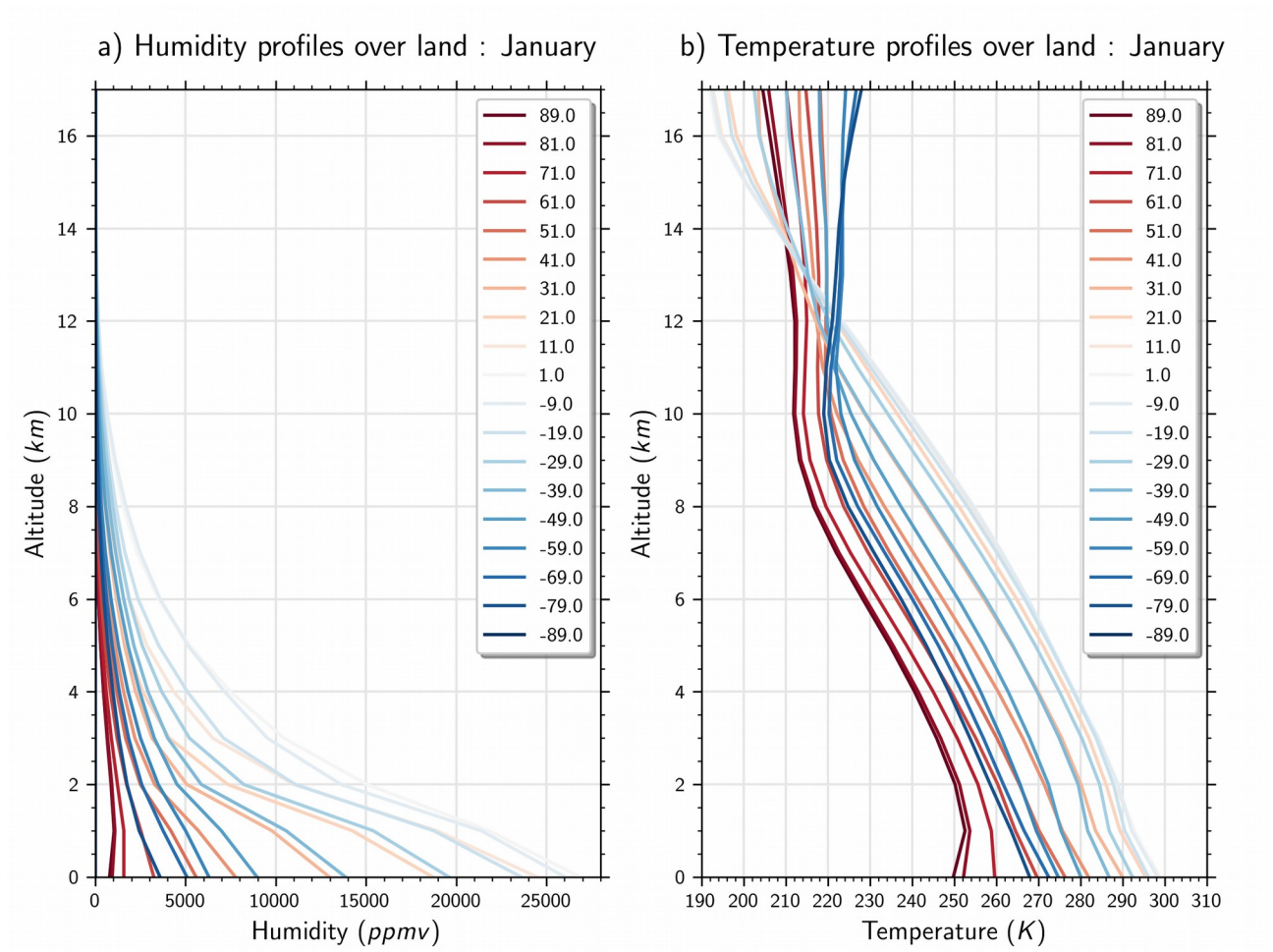
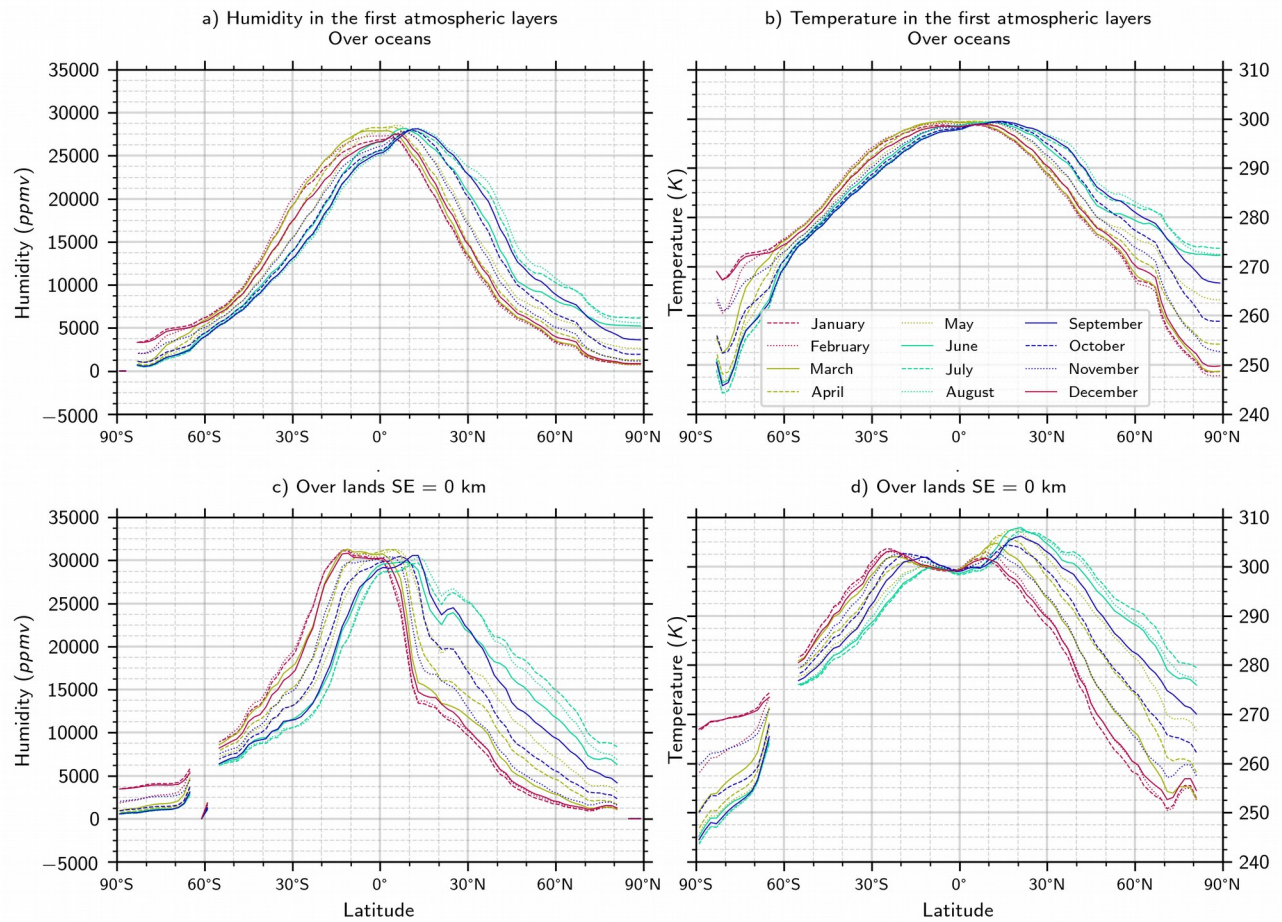
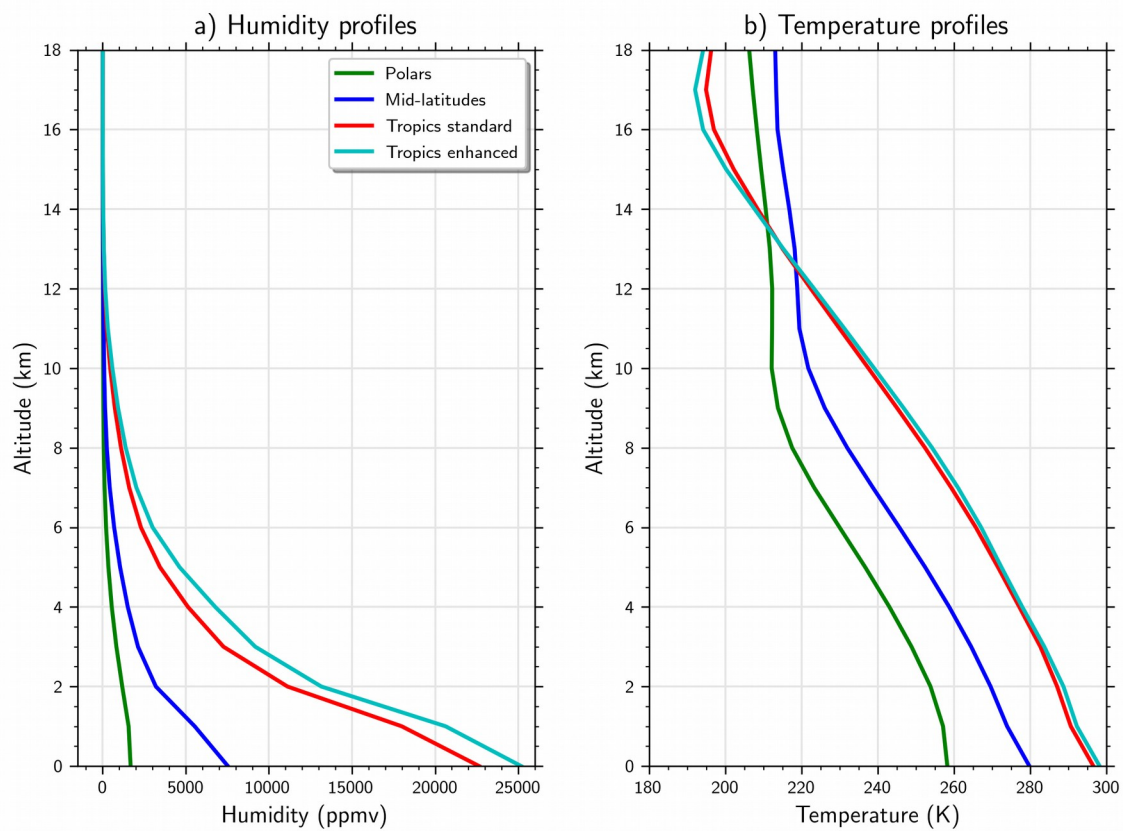


Figure A2: Example of ERA Interim atmospheric profiles taken over land in January and averaged over 10° latitude bands.



**Figure A3: Seasonal and zonal variations of the temperature and humidity in the near surface atmospheric layer ( $Z < 1$  km) from ERA Interim.**



1325 **Figure A4: Annual mean profiles of temperature and humidity from ERA Interim.**



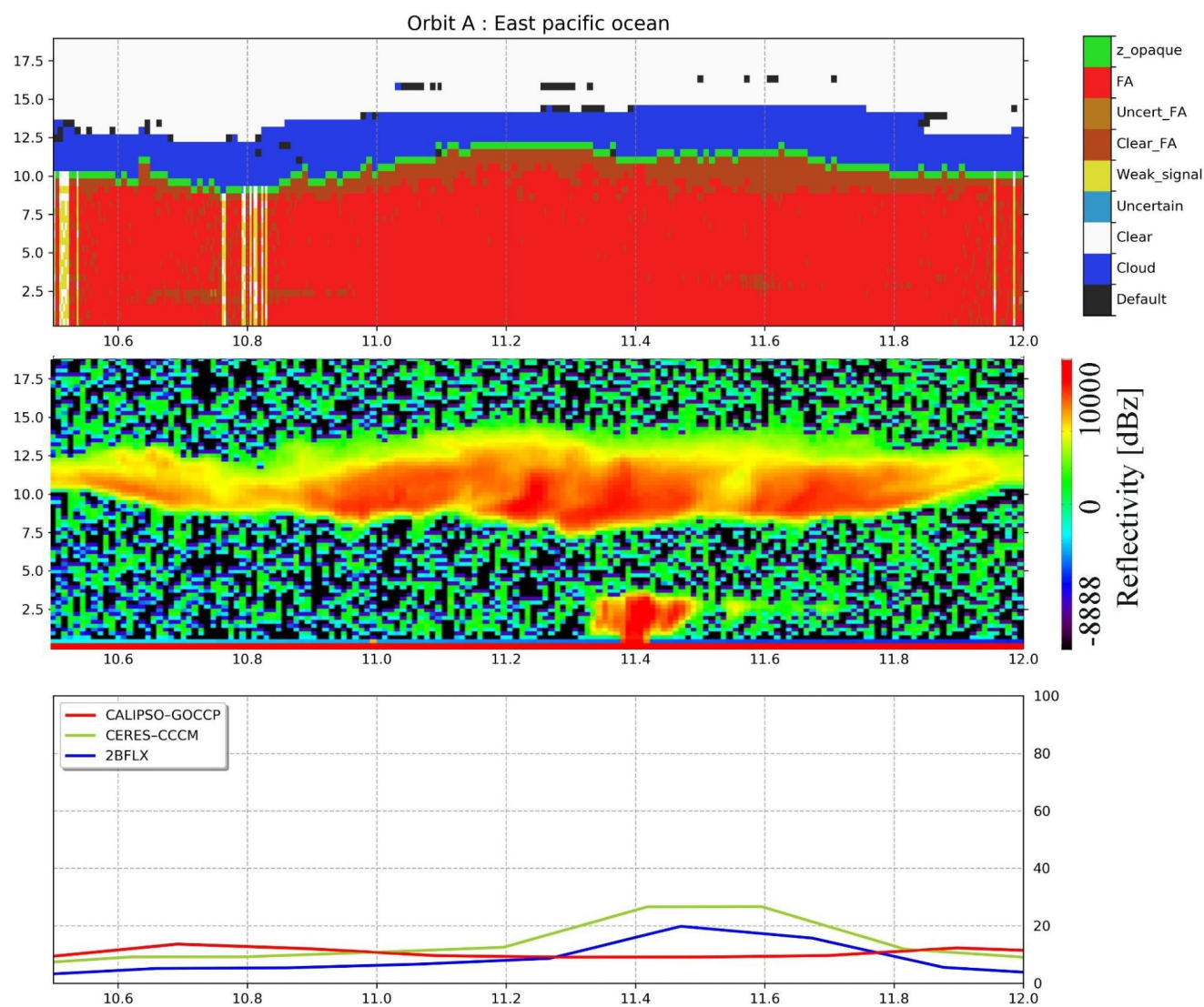


**Figure B1:** same as figure 12.A between 10.5° N and 12 °N : a) CALIPSO-GOCCP-OPAQ mask, b) CloudSat reflectivity and c) surface LW CREs.

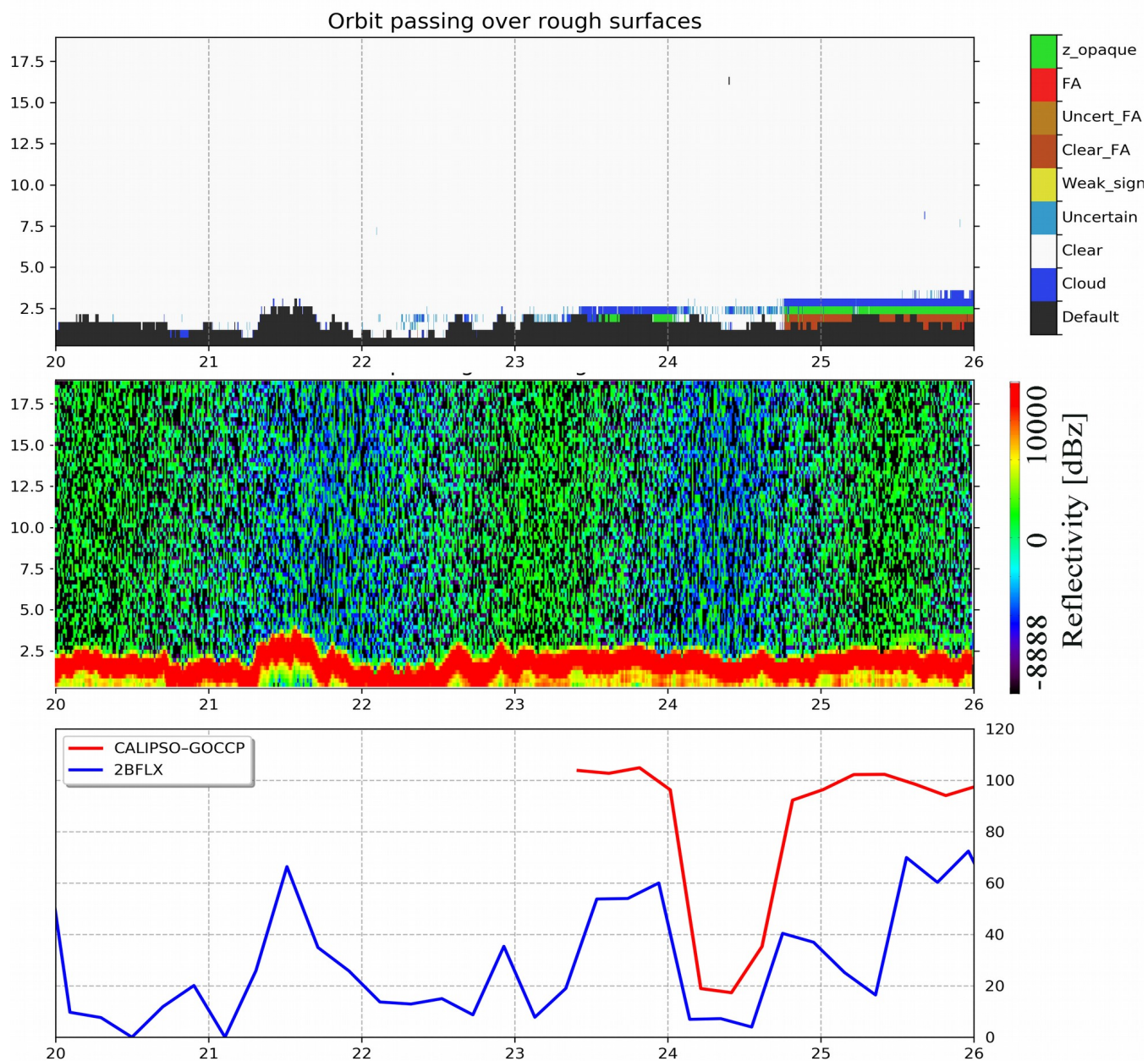
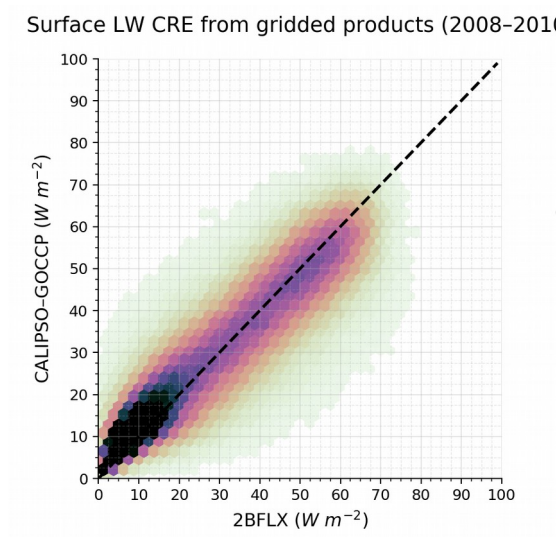


Figure B2: same as fig. B1 but for a piece of orbit passing over China the 10<sup>th</sup> November 2008 at 18 h 58 min 39 sec,

1335

1340

1345



**Figure B3:** Comparison of monthly,  $2^{\circ}\times 2^{\circ}$  gridded surface LW CRE from CALIPSO–GOCCP, and 2BFLX.



		2008/01-2011/04 periode			2008-2015 periode	
		CALIPSO-GOCCP	GOCCP_Z_FA	2BFLX	CALIPSO-GOCCP	GOCCP_Z_FA
Greenland	RMSE	9.0	8.4	16.9	15.9	15.0
	Correlation	0.91	0.95	0.45	0.69	0.70
SIRTA	RMSE	11.0	10.4	15.5	10.8	9.5
	Correlation	0.73	0.73	0.67	0.77	0.77
KWA	RMSE	6.1	5.6	6.9	5.7	4.9
	Correlation	0.03	0.15	0.23	0.08	0.21

**Table 1: Root-mean-square-error (RMSE) and correlation coefficient between satellite products and ground-base observations.**